Structural basis for collagen recognition by the *Streptococcus pyogenes* M3 protein and its involvement in biofilm

Marta Wojnowska[1*#], Takeaki Wajima[2*†], Tamas Yelland[3€], Hannes Ludewig[1¶], Robert M. Hagan[1], Grant Watt[1], Samir W. Hamaia[4], Dominique Bihan[4], Jean-Daniel Malcor[4&], Arkadiusz Bonna[4±], Helena Bergsten[2], Mattias Svensson[2], Oddvar Oppegaard[5], Steinar Skrede[5], Per Arnell[6], Ole Hyldegaard[7], Richard W. Farndale[4±], Anna Norrby-Teglund[2§], Ulrich Schwarz-Linek[1§]

[1]Biomedical Sciences Research Complex, University of St Andrews, North Haugh, St Andrews, KY16 9ST, UK

[2]Center for Infectious Medicine, Karolinska Institutet, Karolinska University Hospital Huddinge, Sweden

[3]CRUK Beatson Institute, Glasgow G61 1BD, UK

[4]Department of Biochemistry, University of Cambridge, Downing Site, Cambridge, CB2 1QW, UK

[5]Department of Medicine, Haukeland University Hospital, Bergen, Norway, Department of Clinical Science, University of Bergen, Norway

[6]Department of Anaesthesiology and Intensive Care Medicine, Sahlgrenska University Hospital, Gothenburg, Sweden

[7]Department of Anaesthesiology, Hyperbaric Medicine Center, Head and Orthopedic Center, Copenhagen University Hospital, Rigshospitalet, Copenhagen, Denmark and Department of Clinical Medicine, University of Copenhagen

* equal contribution first authors

[#] current address: Department of Biochemistry, University of Cambridge, Tennis Court Road, Cambridge, CB2 1QW, UK

[†] current address: Department of Microbiology, Faculty of Pharmacy, Meijo University

[€] current address: Evotec Ltd, 114 Park Dr, Innovation Dr, Abingdon, OX14 4RZ, UK

[¶] current address: Howard Hughes Medical Institute and Department of Biology, Brandeis University, Waltham, MA 02454, USA

[&] current address: Laboratory of Tissue Biology and Therapeutic Engineering, CNRS UMR 5305, University Claude Bernard-Lyon 1 and University of Lyon, 7 Passage du Vercors, 69367 Lyon Cedex 07, France

[±] current address: Triple Helical Peptides Ltd, Cambridge CB22 5DU

[§] corresponding authors, equal contribution senior authors

Acknowledgements

M3-specific antibodies were kindly provided by Professor Gunnar Lindahl, Lund University. We are grateful to Dr Susanne Talay for the M3-encoding pGEX6P-1 vector. The authors thank Dr Conny Yu for preparing a batch of M3-NTD for biofilm experiments. We thank the i04 and i24 beamline staff at the Diamond Light Source synchrotron for their help with data collection.

Funding

This research was funded by the Medical Research Council (MR/N009681/1), grants from European Union FP6 ASSIST (032390) and FP7 INFECT (305340), the Swedish Research Council (2022-01-202), and Region Stockholm, Center for Innovative Medicine (FoUI-975603).

Abstract

The M protein is an essential virulence factor of *Streptococcus pyogenes*, or group A streptococci (GAS), one of the most common and dangerous human pathogens. Molecular and functional characterization of M protein variants and their interactions with host components is crucial for understanding streptococcal pathogenesis and vaccine development. The M3 protein is produced by the prevalent *emm*3 GAS serotype, which is frequently associated with severe invasive diseases. Here we characterize the interaction of M3 with human collagens through detailed structural and biochemical binding analysis. High-resolution structures of the N-terminal M3 domain in the free state as well as bound to a collagen peptide derived from the Collagen Ligands Collection reveal a novel T-shaped protein fold that presents binding sites complementing the characteristic topology of collagen triple helices. The structure of the M3/collagen peptide complex explains how *emm*3 GAS and related streptococci, such as the emerging human pathogen *Streptococcus dysgalactiae* subsp. *equisimilis*, can target collagens to enable colonization of various tissues. In line with this, we demonstrate that the M3/collagen interaction promotes enhanced biofilm formation of *emm*3 GAS in an *emm* type specific manner, which can be inhibited with the recombinant M3 N-terminal domain fragment. Further, *emm*3 GAS, but not an *emm*1 strain, are shown to colocalize with collagen in tissue biopsies from patients with necrotizing soft tissue infections, where GAS biofilms are common. This observation is reproduced in organotypic skin models. Together, these data provide detailed molecular insights into an important streptococcal virulence mechanism with implications for the understanding of invasive infections, strategies for treating biofilm and M-protein based vaccine design.

Introduction

Streptococcus pyogenes (group A streptococcus, GAS) is one of the most prevalent human pathogens. It causes acute diseases ranging from trivial to life-threatening, such as pharyngotonsillitis (strep throat), scarlet fever, impetigo, meningitis, necrotizing fasciitis and streptococcal toxic shock-like syndrome [1]. The highest disease burden is caused by the post-infection sequelae acute rheumatic fever, rheumatic heart disease and glomerulonephritis [2, 3] but there is also a worrying global rise of severe invasive infections [4]. A key virulence factor involved in many if not all these diseases is the GAS M protein. Encoded by the chromosomal *emm* gene, the M protein is covalently anchored at its C-terminus to the cell wall, covering the GAS surface at high density and acting as an adhesin and a potent immune evasion factor [5-7]. M proteins are known, or can confidently be predicted, to form linear fibrils extending approximately 50 nm from the bacterial surface [8, 9]. Their hair-like architecture is based on dimerization of α-helical chains into parallel coiled coils, the defining and dominant structural feature of this class of proteins. Whilst sharing similar overall structure, M proteins are sequentially highly diverse, with over 220 distinct known variants of the *emm* gene defining GAS serotypes [10]. The C-terminal regions of M protein variants are highly conserved and predicted to form well-defined coiled coils. Sequences diverge increasingly towards the N-terminal hypervariable region (HVR) that is projected away from the bacterial surface. Experimental high-resolution structural information for M proteins is limited [11-14].

In addition to their role in adhesion and subverting the host's immune response, M proteins have also been implicated in biofilm formation [15]. Bacterial biofilms are a major cause of difficult-to-treat infections largely contributed by their recalcitrance to antibiotics and immune responses [16]. They are classified as either surface-attached biofilms, typically associated with implants and medical device-associated infections, or non-surface-associated biofilms. The latter are commonly observed in respiratory infections of patients with impaired mucociliary function, and in persistent soft tissue infections seen in chronic wounds resulting from diabetes or impaired vascularization [17]. Biofilm is also a potentially complicating feature associated with severe invasive GAS diseases. Analyses of biopsies collected during the acute phase identified biofilm in over 30% of patients with necrotizing soft tissue infections caused by GAS [18]. Some GAS types, such as *emm*1 and *emm*3, are over-represented among isolates from severe invasive infections, i.e. necrotizing soft tissue infections and streptococcal toxic shock syndrome [1, 19, 20], but no clear association between biofilm formation and *emm* type is known [21]. Köller *et al.* highlighted that the propensity of GAS to form biofilm *in vitro* was directly dictated by the experimental setting where both the medium and coating with specific extracellular matrix proteins influenced the outcome [22].

M proteins have been reported to interact with a wide range of host proteins, such as fibrinogen [23], C4-binding protein [24], plasminogen [25], fibronectin [26], collagens [27] and immunoglobulins [28].

107 Importantly, binding activities vary between *emm* types. Phylogenetic clusters of M proteins broadly
108 share binding propensities [10]. However, very few M protein interactions have been confirmed
109 through biophysical and structural analyses. The M1 protein binds to the fibrinogen D domain in the
110 variable "B-repeat" region [11]. Several M protein types have the ability to bind to the C4-binding
111 protein through their HVRs [14]. While these two molecular complexes rely on the dimeric coiled-coil
112 topology of the M proteins, the plasminogen kringle-2 domain binds to monomeric, non-coiled
113 segments of certain M proteins [29, 30].
114 In a screening of GAS strains belonging to 43 *emm* types, only *emm3* and *emm18* strains were
115 identified by Dinkla *et al.* to bind collagen IV to their surface [27]. For *emm3* isolates, this interaction
116 was demonstrated to depend on direct binding of collagen to the M3 protein. For *emm18* GAS
117 strains, binding was mediated by the hyaluronic acid capsule rather than the M18 protein. Direct
118 collagen binding has also been reported for M1 protein [31]. Based on available evidence collagen
119 binding is not a universal property of GAS M proteins, but appears to be common among M proteins
120 of group C and G streptococci (*Streptococcus dysgalactiae* subsp. *equisimilis*, SDSE) [32, 33], which
121 are emerging as important human pathogens that share disease manifestations and virulence traits
122 with GAS [34, 35].
123 Collagens are commonly targeted by a wide range of pathogenic bacteria for the purposes of tissue
124 colonization and dissemination [36, 37]. They have been shown to interact directly with several
125 bacterial adhesins, such as CNA from *Staphylococcus aureus* [38], YadA from *Yersinia*
126 *enterocolitica* [39], and CNE from *Streptococcus equi* subsp. *equi* [40]. In the latter two cases,
127 adhesin binding has been mapped using the peptide libraries applied in the present study. While the
128 biological role of collagen binding by GAS is unknown, it has been linked to the induction of an
129 autoimmune response associated with post-streptococcal sequelae [27, 41]. The collagen binding
130 site in M3 was mapped to the HVR. A sequence motif that is conserved in related M proteins of
131 group A, C and G streptococci has been identified – the "peptide associated with rheumatic fever"
132 (PARF) [33]. This motif is found in a region predicted to deviate from the canonical coiled coil
133 structure in M3, several other M proteins and their homologs in non-group A streptococci (Figure 1).
134 Binding of M3 protein to other collagen types has not been reported, but the M protein FOG (aka
135 Stg11) of SDSE was found to bind to collagens I and IV [33, 42].
136 To gain insights into mechanism and biological role of streptococcal collagen binding, we
137 characterised the interaction of M3 with the Collagen Ligand Collections (CLCs, triple-helical
138 collagen peptide libraries formerly known as Toolkits), and determined crystal structures of the M3
139 N-terminal domain (M3-NTD), encompassing the HVR, alone and in complex with a CLC-derived
140 collagen peptide. We find that M3-NTD folds into a novel T-shaped domain that binds promiscuously
141 to collagen triple helices. Furthermore, we demonstrate that the M3-collagen interaction underpins
142 biofilm formation by GAS *emm3* isolates from necrotizing soft tissue infections, which can be
143 inhibited *in vitro* by recombinant M3 protein and collagen peptides.

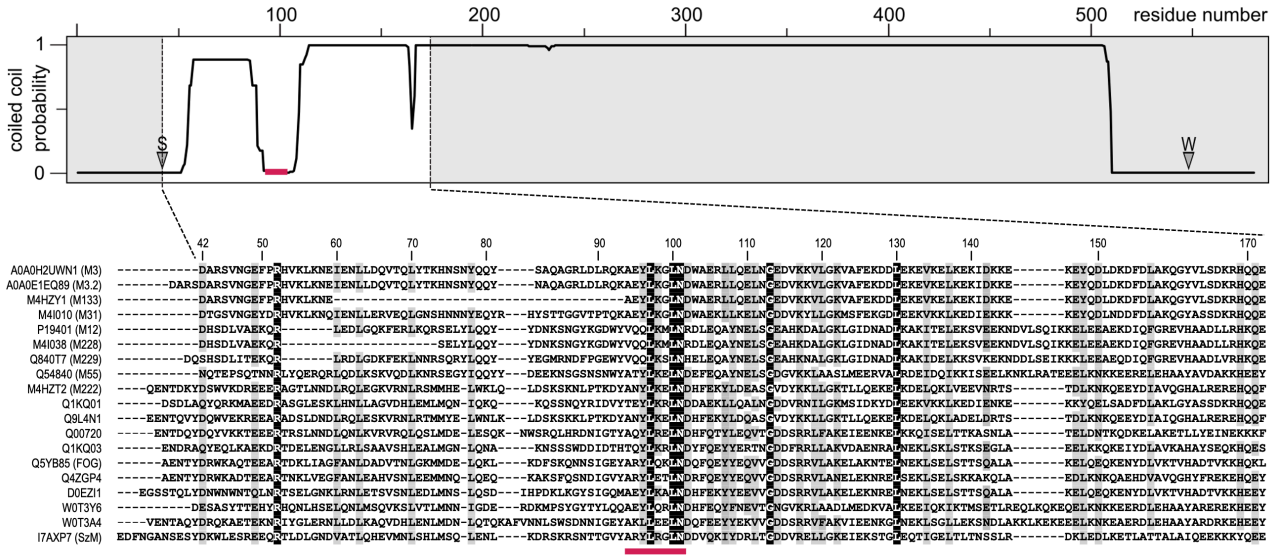

Figure 1. Multiple sequence alignment of the hypervariable regions of streptococcal M proteins. The top panel shows a MARCOIL coiled coil prediction [43] for full-length M3 protein. Positions of signal and wall anchor cleavage sites are indicated by S and W, respectively. The PARF motif (position indicated by pink bar), previously suggested to be required for collagen binding, resides in a region of M3 that is predicted to not adopt coiled coil topology. In the alignment, sequence similarity is indicated by grey shading for residues conserved or similar in at least 75% of sequences. 100% conserved residues are highlighted by black shading. Uniprot identifiers are shown to the left of the alignment. Sequences are ordered by alignment score. The proteins are from the following species: *Streptococcus pyogenes*: A0A0H2UWN1 (M3), A0A0E1EQ89 (M3.2), M4HZY1 (M133), M4I010 (M31), P19401 (M12), M4I038 (M228), Q840T7 (M229), Q54840 (M55), M4HZT2 (M222); *Streptococcus dysgalactiae* subsp. *equisimilis*: Q1KQ01, Q9L4N1, Q00720, Q1KQ03, Q5YB85, Q4ZGP4, D0EZI1, W0T3Y6, W0T3A4; *Streptococcus equi* subsp. *zooepidemicus*: I7AXP7.

Results

Recombinant M3 protein binds to the triple-helical domain of collagens II and III

The first aim of this study was to confirm the collagen binding activity of streptococcal M3 protein, and to identify any specific binding sites in collagen. To reduce the complexity of the experimental system we chose collagens II and III, as these are homotrimers, in contrast to, for instance, heterotrimeric collagens I and IV [44]. Recombinant M3 protein, lacking the N-terminal secretion signal and the C-terminal membrane-spanning region was produced in *Escherichia coli* as a glutathione S-transferase (GST) fusion protein. Binding to collagens II and III was investigated using CLCs, libraries of 56 and 57 overlapping triple-helical peptides, respectively, covering the entire triple-helical tropocollagen domain of these two collagen types (1014 and 1029 amino acids) [45].

170 Recombinant M3 was found to bind to CLC peptides to various degrees, as quantified by an ELISA-
171 like approach using an anti-GST antibody (Figure 2). While there were clear differences in binding
172 between the CLC peptides, it was impossible to identify sequence features that were conserved in
173 good binders (high apparent affinity) but absent from peptides that gave rise to signals comparable
174 to negative controls. Neither sequence motifs, nor composition of the peptides (e.g., presence of
175 hydroxyprolines, charged, hydrophobic or aromatic residues) were distinct in good binders. To
176 investigate further the sequence requirements for M3 binding, we ranked the CLC peptides in
177 decreasing apparent affinity, measured as A_{450} determined in the solid-phase binding assay, and
178 then analyzed the distribution of particular amino acids in the entire set, pooling data from CLC-II
179 and CLC-III. After background subtraction, we defined three binding groups: high affinity, having A_{450}
180 between 0.5 and 0.75; medium affinity, A_{450} from 0.25 to 0.5; and low affinity, A_{450} from 0 to 0.25.
181

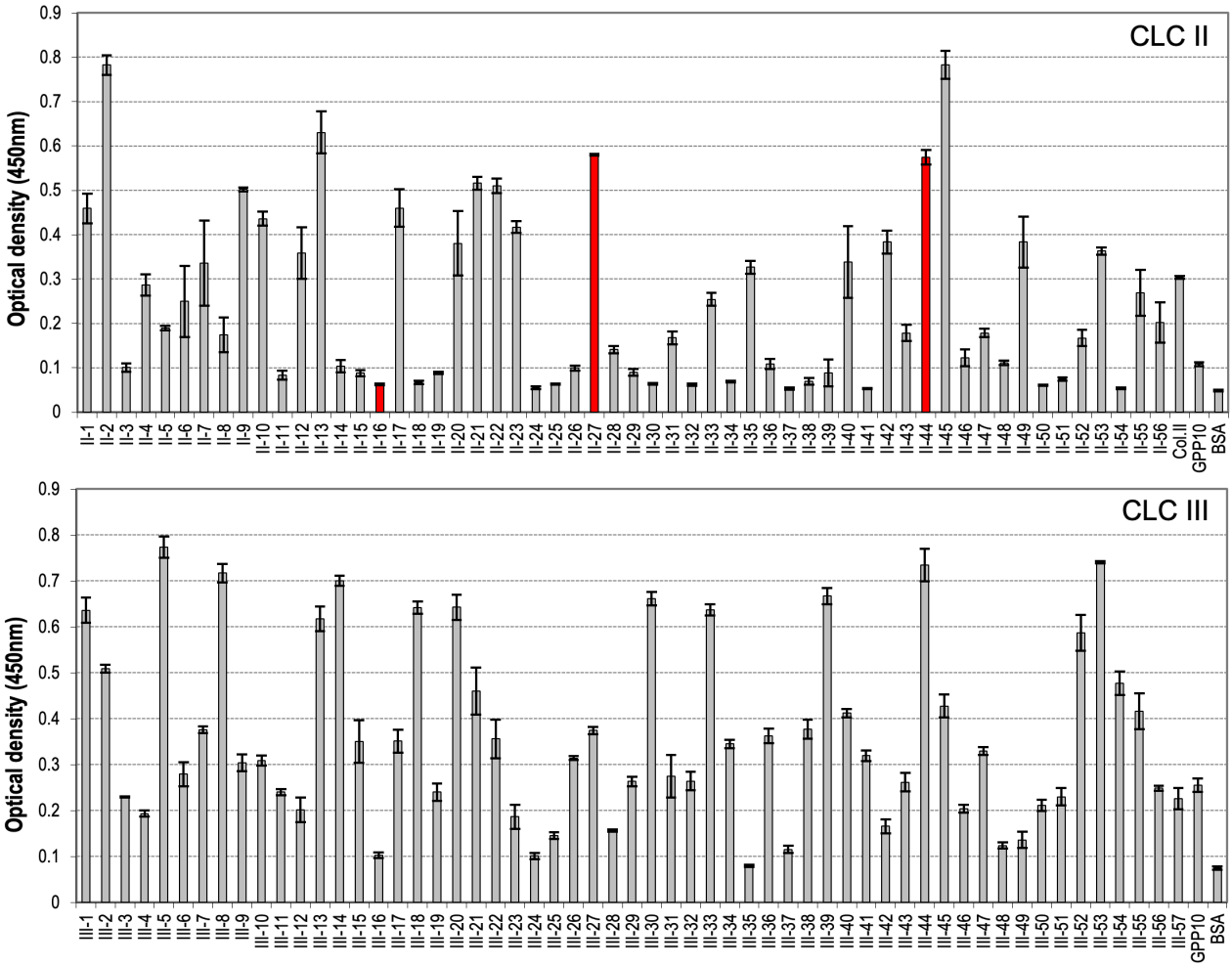

182

183 Figure 2. Binding of full-length M3 protein fused to GST to immobilised CLC II and III peptides. ELISA
184 signal based on GST antibody is plotted against peptides spanning the tropocollagen (triple-helical)
185 regions of collagens II and III, as well as positive (collagen II) and negative (GPP10, BSA) controls.
186 Signals for three peptides chosen for further binding experiments are highlighted in red.

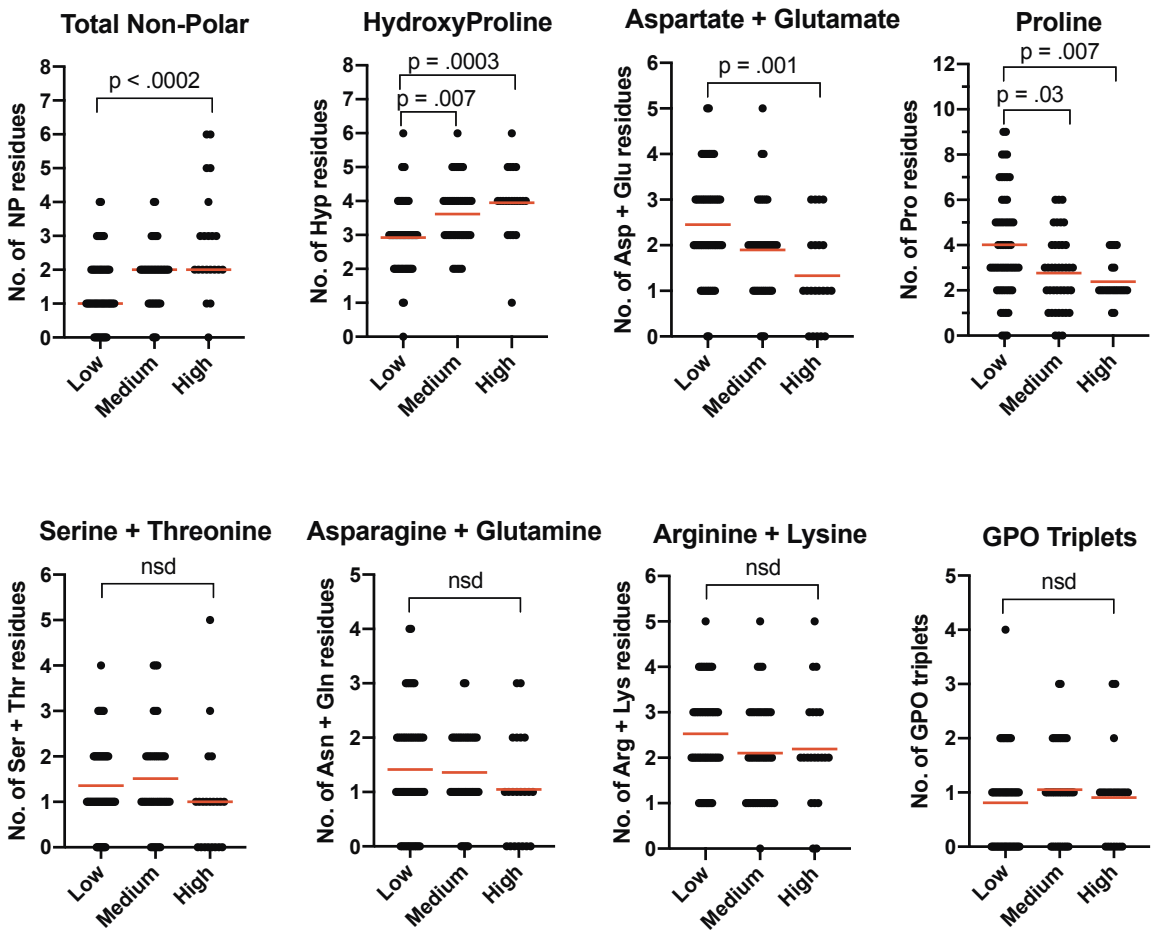

Figure 2—figure supplement 1: The Figure shows the number of specific residues or residue classes per CLC peptide (y-axis) plotted versus rank group (x-axis). Groups are defined as low affinity (A450 = 0 to 0.25), medium affinity (A450 = 0.25 to 0.5) and high affinity (A450 = 0.5 to 0.5) in the solid phase binding assays. Statistical difference between numbers in each group was determined by non-parametric testing as defined in Methods.

We counted residues of each type in these three groups and compared their occurrence in peptides of the three binding groups using non-parametric tests (Figure 2—figure supplement 1). The outcomes are summarized in Table 1. Hydrophobic amino acids and hydroxyprolines appear to be more frequent in good binders, while prolines and acidic residues are underrepresented. The negative effect of proline on binding may explain why the $[GPP]_5$ flanking sequences of the CLC peptides do not dominate binding to M3, allowing marked sequence selectivity to be observed in the binding assays.

205 Table 1: Effect of amino acid classes on binding of M3 to CLCs.

Amino Acid class	Effect on binding rank	Significance
Hydrophobic (F, L, V, M, I)	Positive	p = .0002
Hydroxyproline (O)	Positive	p = .0003
Polar (S, T)	None	
Polar (Q, N)	None	
Basic (R, K)	None	
GPO triplets	None	
Acidic (D, E)	Negative	p = .001
Proline (P)	Negative	p = .0007

206

207 ***M3-NTD harbors the collagen binding site***

208 Full-length M proteins are not amenable to high-resolution structural characterization due to their
209 anisotropic shape and potential conformational dynamics. We therefore designed a construct
210 representing the M3 N-terminal domain (M3-NTD), which comprises the HVR and a short region
211 predicted to adopt a dimeric coiled-coil structure. This fragment would not only allow structural
212 characterization but could also be used to confirm the previously suggested localization of the
213 collagen binding site at the HVR [33]. M3-NTD includes the 110 N-terminal residues of mature M3
214 (residues 42-151 of the M3 protein precursor sequence). To stabilize a dimeric conformation, Leu151
215 was replaced with a cysteine for disulfide bond formation at the C-terminus. Leu151 is predicted to
216 occupy a "d" position in the canonical coiled coil heptad pattern, forming part of the hydrophobic
217 interface between the α-helices, a position ideally suited for disulfide bond formation [46]. A ^{15}N
218 isotopically labelled version of M3-NTD was made for NMR spectroscopic analysis. From a
219 comparison of ^{1}H, ^{15}N heteronuclear single-quantum coherence (HSQC) spectra it is evident that a
220 significant structural change occurred upon oxidation (resulting in disulfide bond formation) of the
221 protein. The higher dispersion of signals, most noticeably in the ^{1}H dimension, indicates disulfide-
222 linked M3-NTD adopts a folded conformation (Figure 3A). In contrast, the reduced, monomeric form
223 gives rise to a poorly resolved spectrum with signals falling within the random-coil chemical shift
224 range, and big differences in crosspeak intensities that suggest dynamic behavior (Figure 3B). This
225 demonstrates the C-terminal disulfide bond is required to stabilize a dimeric, folded structure that
226 differs from extended unfolded or linear α-helical conformations.

227 To test if M3-NTD harbors the collagen binding site, binding to selected CLC triple-helical peptides
228 was studied by isothermal titration calorimetry (ITC). We selected two peptides that showed medium
229 to high apparent affinity in the CLC screening (II-27 and II-44) and a low affinity peptide (II-16). These
230 three peptides all interacted with M3-NTD in solution (Figure 4A-C). II-27 and II-44 binding was
231 characterized by dissociation constants (K_D) in the low micromolar range (7 and 5 μM, respectively).
232 II-16 had an approximately ten times lower affinity (K_D = 70 μM) for M3-NTD. These K_Ds reflect the

differences in binding of full-length M3 evident from the CLC solid-phase binding assay. Fitting of the sigmoidal binding curves for II-27 and II-44 suggested binding of one triple-helical peptide per M3-NTD monomer, i.e., two indistinguishable collagen binding sites per M3 dimer. To assess if the interaction was dependent on the triple-helical conformation of the CLC peptides, we titrated M3-NTD into a monomeric version of II-44 with scrambled GPP repeat sequences at the termini [47]. No binding was observed (Figure 4D).

In conclusion, the collagen binding site of M3 was confirmed to reside in M3-NTD. CLC solid-phase binding results obtained for full-length M3 align with in-solution interaction analyses by ITC using M3-NTD. Binding of M3-NTD to collagen peptides depends on their triple-helical structure.

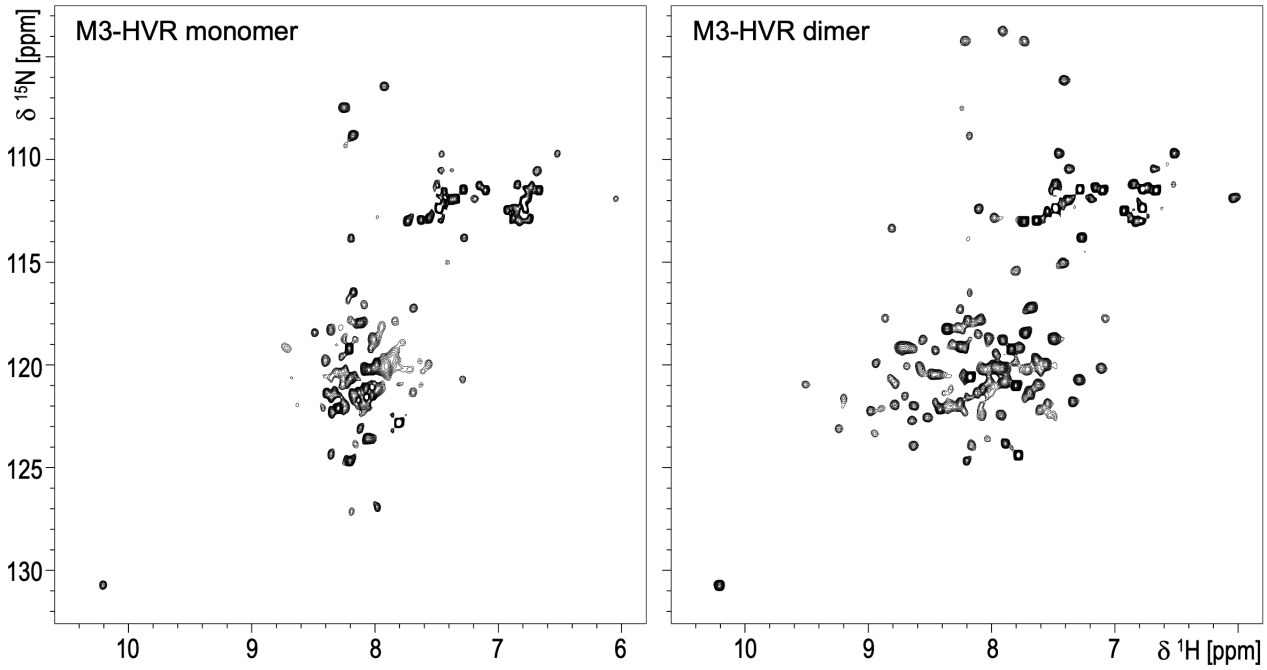

Figure 3. $^{1}H,^{15}N$ HSQC spectra for monomeric and disulfide-bond stabilized dimeric M3-NTD.

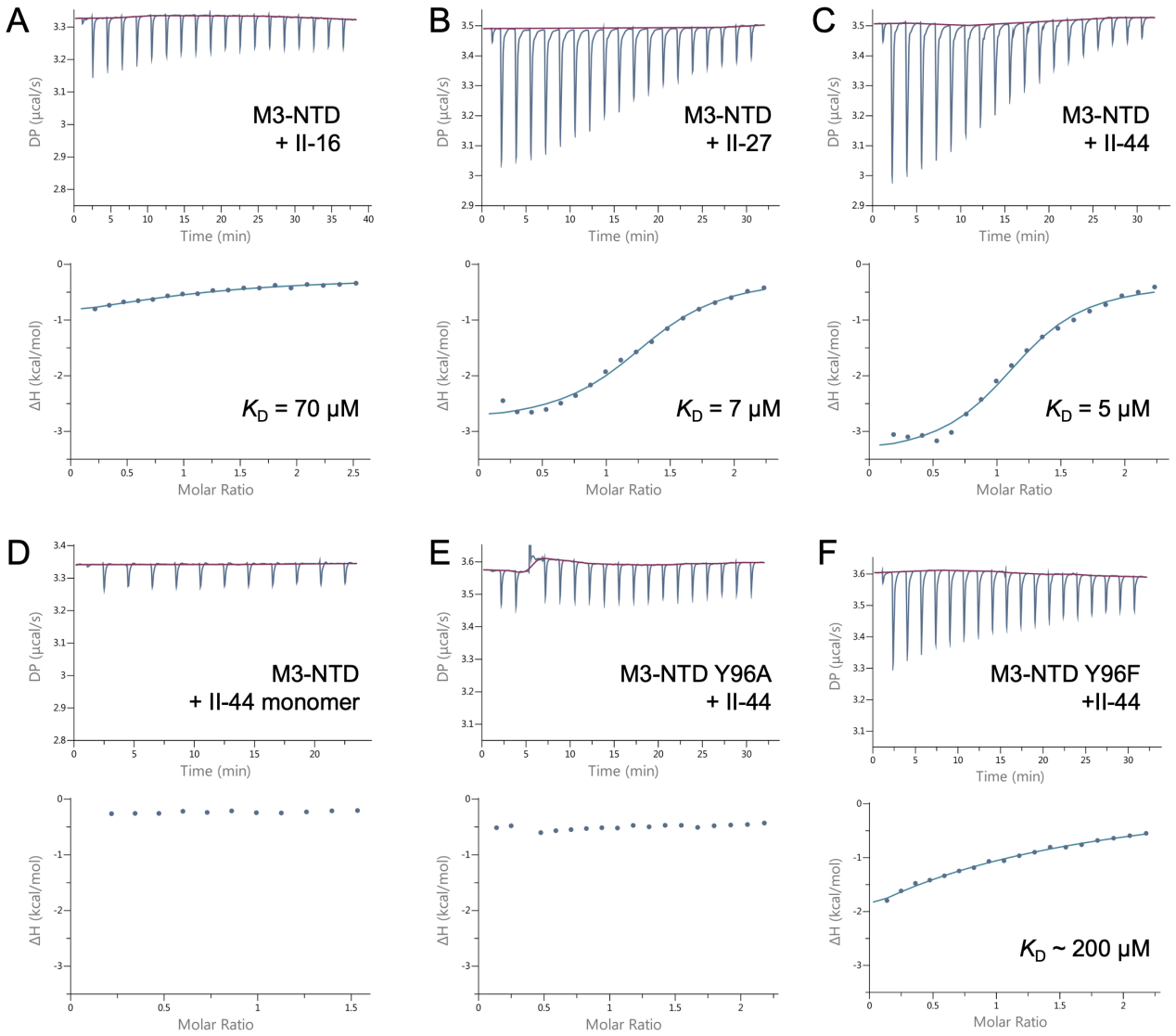

Figure 4. ITC binding curves for M3-NTD interactions with CLC peptides. Top panels show heat responses to repeated injections of M3-NTD into collagen peptide solutions, with baselines shown in red. Bottom panels shown integrated signals (enthalpy changes) plotted against the molar ratio of binding partners. Where non-linear fitting gave meaningful results, the fits are shown as blue lines, and dissociation constants (K_D) are specified.

M3-NTD adopts a folded structure deviating from dimeric coiled coil

M3-NTD crystallized in several conditions with the best crystals diffracting X-rays to a resolution of 1.9 Å at the synchrotron radiation source. Phasing and structure determination was achieved using a selenium single-wavelength anomalous diffraction (Se-SAD) dataset at 2.6 Å resolution with the final model refined against the native data set at 1.9 Å resolution (Table 2).

M3-NTD is a symmetrical homodimer, linked at the C-terminus by a disulfide bond (Figure 5A). The first three residues of the construct (Gly-Ala-Met), a cloning artefact, are not resolved in the structure.

261 Table 2: Data collection and refinement statistics

	M3-NTD	**SeMet M3-NTD**	**M3-NTD+JDM238**
Data collection	**8P6K**		**8P6J**
Spacegroup	C2	C2	P1
Cell dimensions			
a, b, c (Å)	150.5, 24.1, 78.0	150.4, 25.1, 77.0	31.8, 51.5, 80.2
a, b, c (°)	90, 105.3, 90	90, 104.4, 90	87.3, 84.8, 89.4
Resolution (Å)	37.62 - 1.92 (1.94 - 1.92)	37.3 – 2.67 (2.71 – 2.67)	79.77 - 2.32 (2.45 - 2.32)
R_{meas}	0.058	0.198	0.107
I/σ	14.8	10.2	2.1
$CC_{1/2}$	0.9	1	1
Completeness (%)	97.80 (94.07)	98.8	89.58 (89.66)
Multiplicity	6.2	18.6	1.7
Refinement statistics			
Resolution (Å)	37.6 - 1.92		79.77 - 2.32
No. reflections	21390 (691)		19527 (2819)
R_{work}/R_{free}	0.230/0.268		0.241/0.285
Ramachandran favoured (%)	97.7		97.7
Ramachandran outliers (%)	0		0.5
RMS deviations			
Bond lengths (Å)	0.039		0.013
Bond angles (°)	2.06		1.89

262

263 The fold represents a novel T-shaped architecture with no significantly similar structures identifiable
264 by the protein structure comparison server DALI [48]. Each monomer is composed of three α-helices,
265 H1-H3. The H3 helices comprise the C-terminal 38 residues of M3-NTD (M3 residues 114-151) and
266 form a coiled coil stem. This, in the full-length protein, would be extended into a ~50 nm long coiled
267 coil characteristic of M proteins (Figure 5B). Helices H1 and H2 form hairpins that pack against each
268 other to form the slightly kinked bar of the T-shape, effectively a three-helix bundle. A key residue is
269 Gly113, which resides at the T-junction, separating H2 and H3 (Figure 5C). It is completely
270 conserved in M proteins identified in our sequence similarity search (Figure 1). The T-junction
271 structure is defined by conserved leucine and isoleucine residues that form a small hydrophobic core
272 (Figure 5C). The T-bar structure is stabilized by a network of polar interactions of several conserved
273 residues, most notably inter-chain salt bridges of Arg52 with Asp102 and Glu105, and an inter-chain
274 hydrogen bond between the side chains of Glu49 and Asn101 (Figure 5D). Asn101 is one of the
275 completely conserved residues in the PARF motif, previously implicated in collagen binding. This
276 motif is located on H2 at the bottom of the T-bar (Figure 5A). Some but not all conserved PARF
277 residues contribute to the formation of the T-bar structure of M3-NTD. Leu97 and Asn101 are the
278 only completely conserved residue of PARF with a structural role. Leu97 is buried at the interface
279 between the H1-H2 hairpin of one monomer and H1 of the other monomer, packing against the
280 Tyr81 sidechain (Figure 5D).

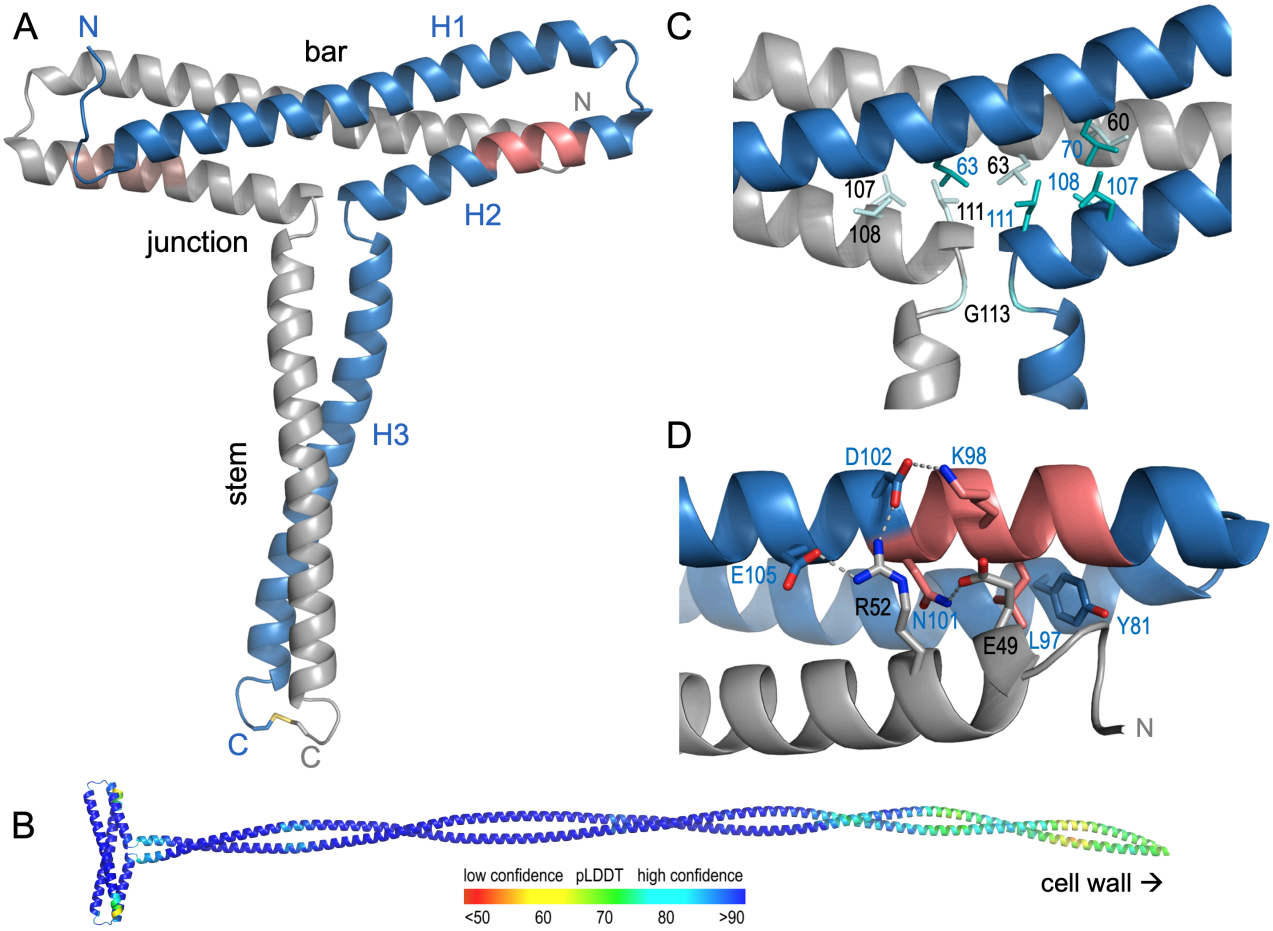

Figure 5. Crystal structure of M3-NTD (PDB 8p6k). A) Ribbon diagram of the covalently stabilized M3-NTD dimer. Monomers are shown in blue and grey. The regions previously associated with collagen binding (PARF motif) are highlighted in red. N-termini (Asp42) and C-termini (Cys151) are labelled N and C, respectively. The three helices of the blue monomer are labelled H1-3. The C-terminal disulfide bond is shown as sticks. B) Ribbon diagram model for the full extracellular region of M3, predicted by AlphaFold3 [49] and colored by per-residue confidence (pLDDT). C) Conserved leucine, isoleucine (Ile60) and glycine (Gly103) residues define the T-junction structure of M3-NTD. D) Role of conserved residues around the PARF motif in stabilizing the T-bar region of M3-NTD. Polar contacts are shown as dashed lines.

An N-terminal T-shaped fold is predicted to be a feature of other M proteins

AlphaFold3 [49] predictions were carried out for the proteins identified in our sequence similarity search (Figure 1) to support the structural role of the conserved residues. In validation of this approach, the AlphaFold3 predicted model of M3 is almost perfectly superimposable with the experimental M3-NTD structure (Figure 6A). All other proteins included in this study are predicted to have T-shaped N-terminal domains, with exception of proteins M133 and M228, where deletions break the topology of the T-bar fold (Figure 6B, Figure 6—figure supplement 1). Some of the

predictions for GAS M protein variants, such as M12 and M55, carry low confidence and may well not adopt the T-fold. HVRs of M proteins that are phylogenetically more distant to M3, such as M1 and M28, are not predicted to fold into any distinct tertiary structure deviating from coiled coil (Figure 6C). On the other hand, M proteins of SDSE and the SzM protein of *Streptococcus equi* subsp. *zooepidemicus* (SESZ) are predicted with high confidence to adopt a structure similar to M3. This analysis structurally validates our sequence alignment of M3 homologs. It suggests the T-shaped structure of the NTD is a feature of a subclass of M proteins and is common in SDSE.

M3-NTD binds promiscuously to the collagen triple helix

M3-NTD is a structurally tractable fragment that retains the collagen binding activity of the full-length protein. We chose II-27, a CLC peptide with good affinity for M3-NTD, as the basis for structural characterization of an M3-collagen complex. II-27 contains an atypical $\alpha 1\beta 1$ integrin-selective motif, GVOGEA [50]. To increase chances of crystallization, a shorter 24-residue peptide, JDM238, was synthesized which contains the GVOGEA motif flanked by three glycine-proline-4-hydroxyproline

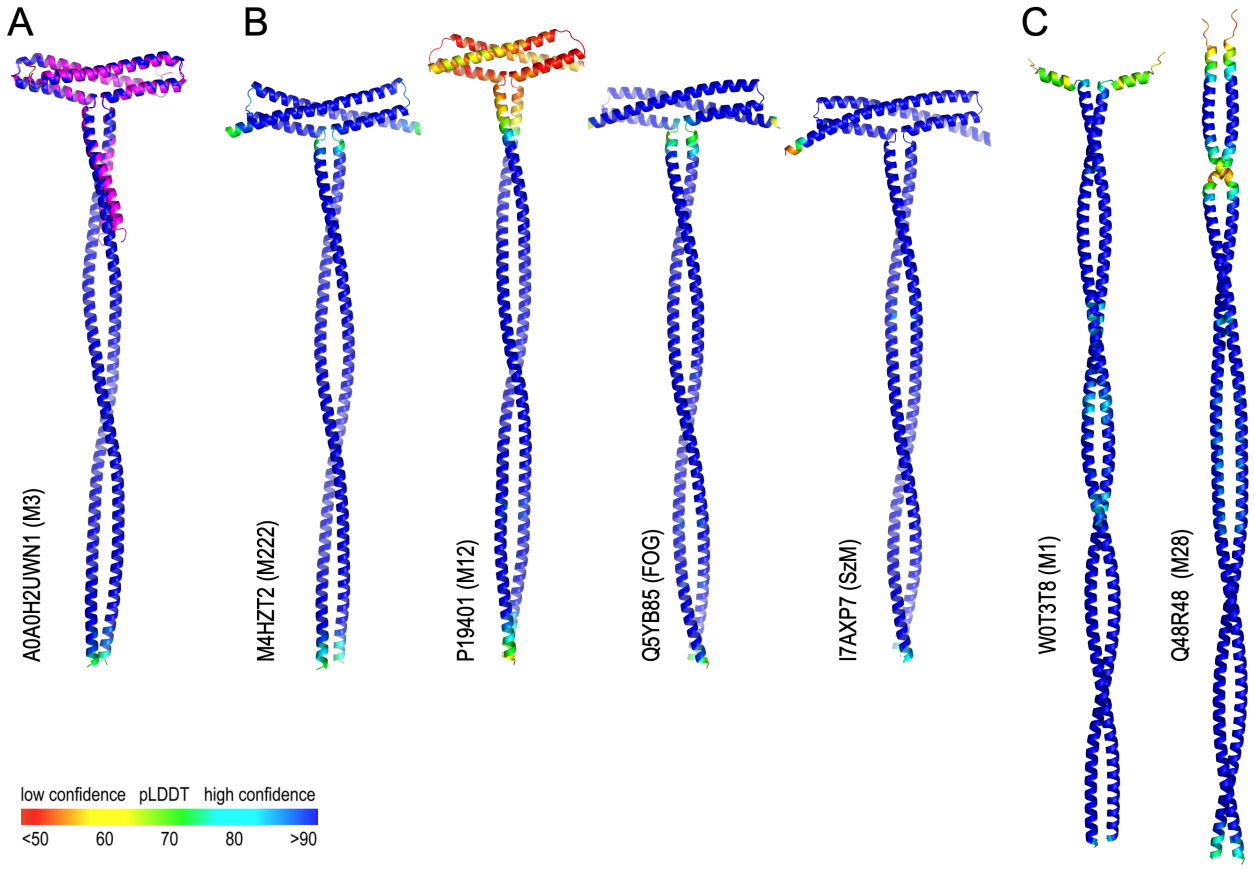

Figure 6. AlphaFold3 predictions for M proteins of GAS, SDSE and SESZ. A) Overlay of the experimental M3-NTD structure (magenta) with a predicted structure for the N-terminal 230 residues of mature M3 (coloured by pLDDT). B) Predicted structures for the N-terminal 230 residues of other M proteins included in the sequence alignment (Figure 1). C) Predicted structures for the N-terminal 230 residues of M1 and M28 proteins, which are not known to interact with collagens.

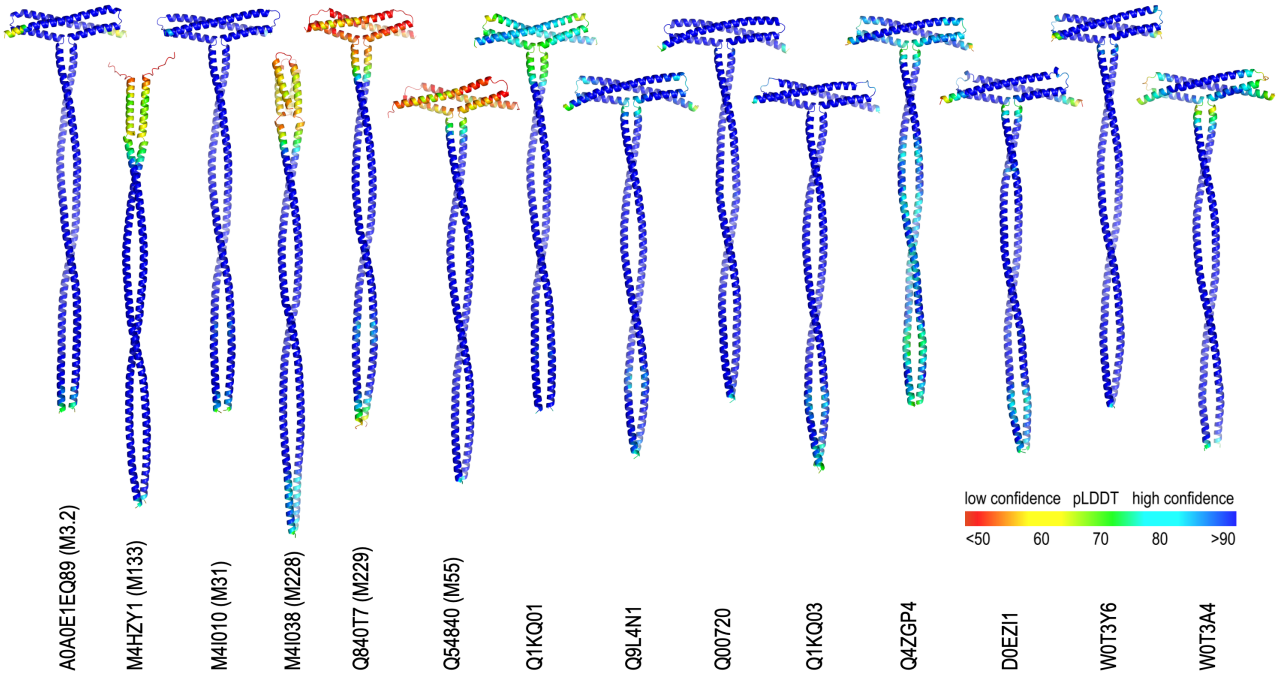

Figure 6—figure supplement 1. Additional AlphaFold3 predicted structures of proteins included in the sequence alignment (Figure 1). The N-terminal 230 residues of mature proteins were included in predictions (colored by pLDDT). For M133 only the first 196 residues have been modelled to highlight of the effect of the deletion of residues that are integral to the T-shape structure of M3.

(GPO) repeats at each terminus. Crystals formed in conditions containing JDM238 and M3-NTD at a 1.5:1 ratio and diffracted synchrotron X-rays to 2.3 Å resolution. Molecular replacement with M3-NTD yielded a high-quality structural model for the complex (Table 2).

In agreement with our ITC data for CLC II-27 binding to M3-NTD, the M3-NTD dimer is bound to two copies of triple-helical JDM238. While both copies occupy equivalent binding sites on opposite faces of the M3-NTD T-bar, they contact the protein with two different regions (Figure 7). One copy contacts M3-NTD through residues 15-21 of the C-terminal GPO repeats, the other is bound at its more central GPOGVO region (residues 6-12) (Figures 7 and 8A). The presence of two different binding registers in the same crystal is likely an effect of crystal packing, but it also reflects a lack of specificity of collagen binding by M3, in line with the CLC screening data. Superposition of the two binding sites highlights how the M3-NTD T-bar complements the characteristic and uniform surface topology of triple helices in both binding registers in the same fashion (Figure 8B).

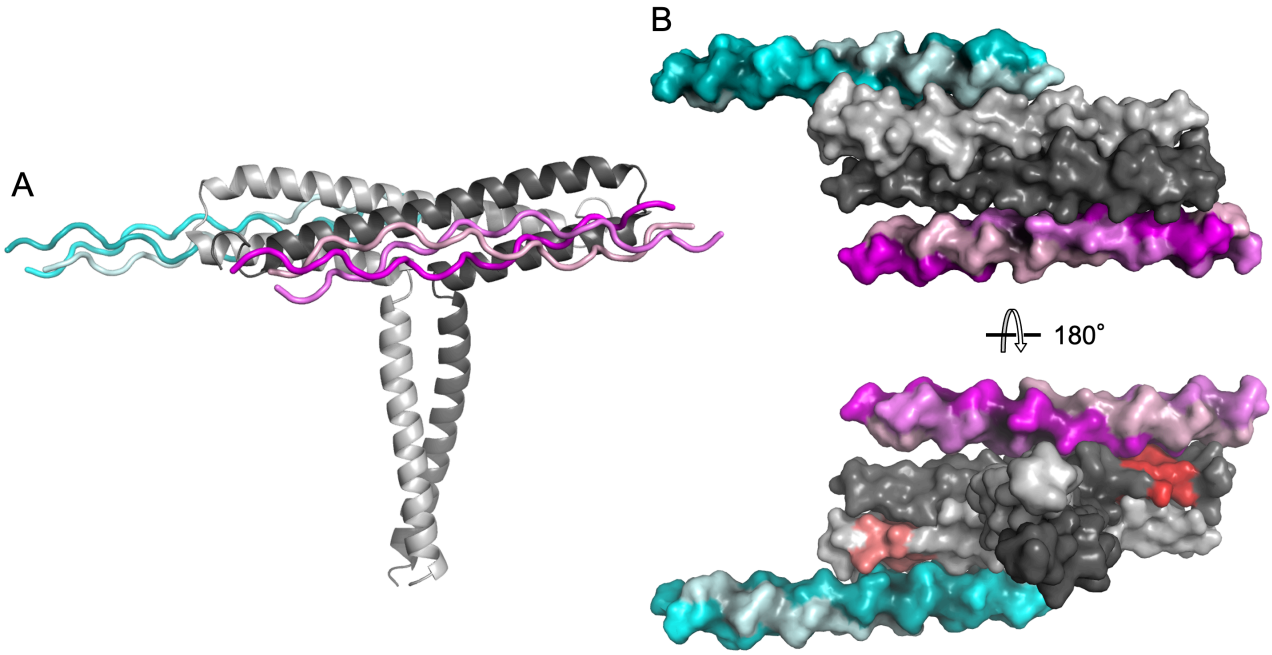

Figure 7. Structural basis of collagen binding by M3 (PDB 8p6j). A) Crystal structure of the complex of M3-NTD (subunits shown in light and dark grey cartoon representation) with collagen-derived peptide JDM238. Two binding registers are observed bound to equivalent sites of the M3-NTD dimer, indicated by shades of magenta and cyan. B) Space-filling models of views from the top of the T-bar of M3-NTD (top) and looking down the stem towards the bottom of the T-bar (bottom). The PARF motif is shown in tones of red, otherwise coloring is as in A.

The M3 collagen binding site includes the PARF region on H2 (residues 94-101), extending beyond it to include the C-terminal half of H1 and most of H2 (Figure 8). This confirms previous reports on the involvement of PARF in collagen binding [32, 33]. Interfaces between the binding partners largely comprise hydrophobic interactions between highly complementary surfaces. M3 residues Tyr96 and Trp103 play prominent roles: they pack against Hyp and Pro sidechains, filling grooves on the collagen triple helices and form polar contacts with the peptide backbone. The indole amino group of Trp103 interacts with the carbonyl of Ala15 or Hyp6 (depending on the register), while Tyr96 forms a water-mediated hydrogen bond with the carbonyl of Hyp9 or Hyp18. In one binding mode, M3 Gln42 hydrogen bonds with the same water molecule as Tyr96. Direct polar contacts also include M3 residues Lys35 and Arg49 which interact with the hydroxyl group of Hyp9 and the backbone carbonyl of Hyp12, respectively. In addition, in one binding mode M3 residue Gln46 forms a hydrogen bond with Gly22 of the peptide via a water molecule.

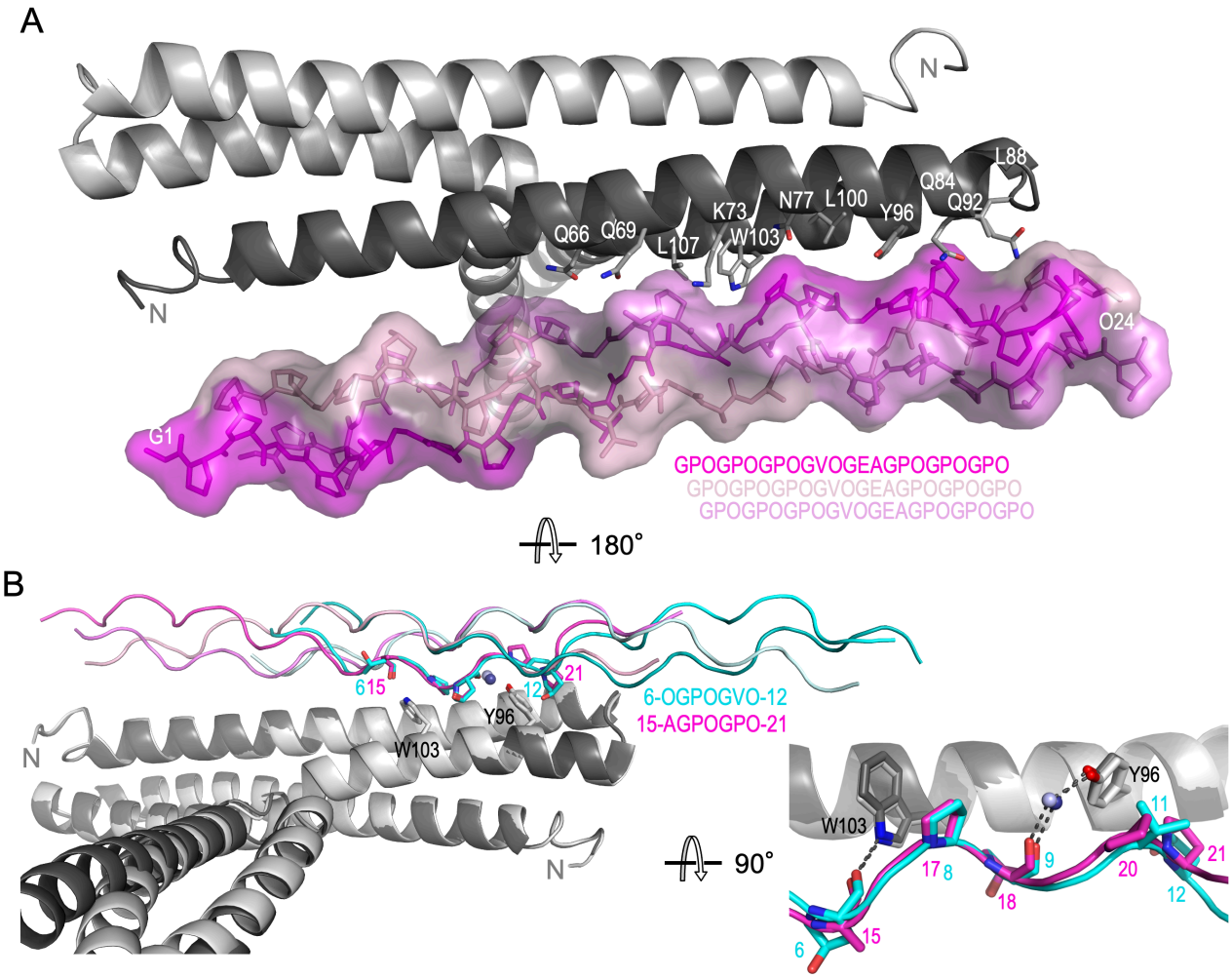

Figure 8. Collagen triple helix/M3-NTD interface. A) Residues of M3-NTD (grey cartoon representation) that form the collagen binding site are shown as sticks and are labelled. The collagen peptide triple helix is shown in stick and surface representation in shades of magenta. The sequence is shown indicating the staggered arrangement of the chains in the triple helix. B) Superposition of the two peptide binding sites to highlight conservation of collagen binding mode despite sequence deviation between the two binding registers. Tyr96 and Trp103 are shown as sticks. The two monomers of M3-NTD are shown in light and dark shades of grey. Collagen peptides of the two binding modes are shown in magenta and cyan, with five equivalent sidechains shown as sticks. The equivalent sequences of the binding sites are shown. Water molecules in the binding interface are shown as blue spheres. In the zoomed-in image on the bottom right, only one of the collagen peptide chains is shown per complex for clarity. Hydrogen bonds are shown as grey dashed lines.

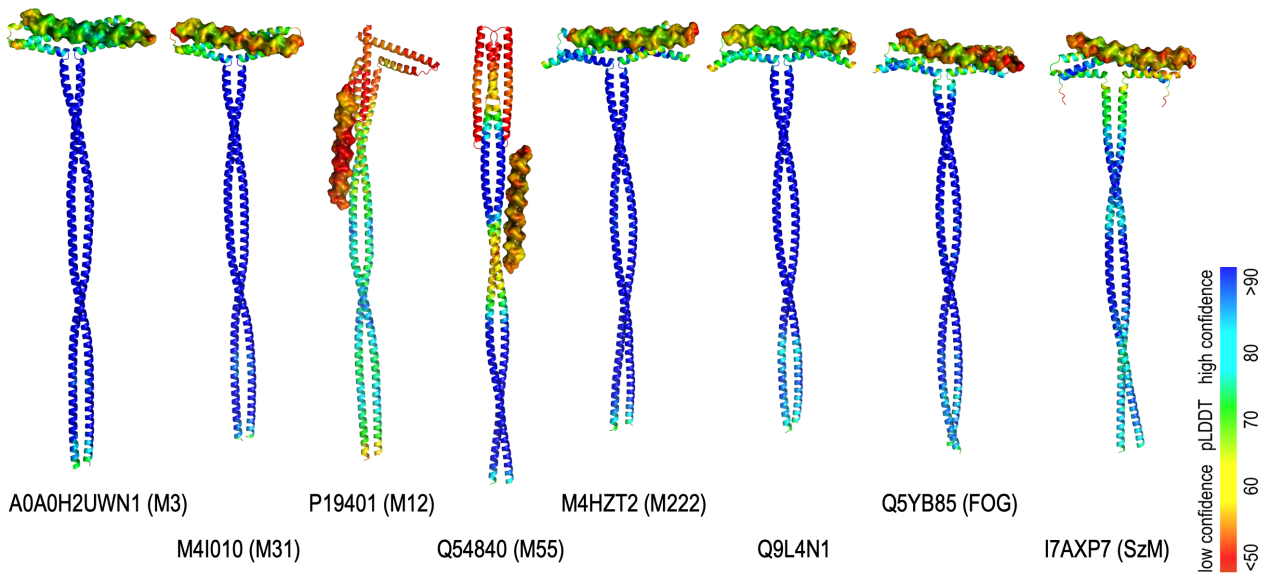

Figure 8—figure supplement 1: AlphaFold3 predicted structures of M proteins in complex with a model collagen peptide (GPO_8). Two chains of the N-terminal 230 residues of mature proteins and, for clarity, only three collagen peptide chains were included in predictions. M proteins are shown in cartoon, GPO_8 peptide in surface representations, respectively (coloured by pLDDT).

Tyr96 is a conserved residue of the PARF motif. We tested its role in collagen binding using two site-specific variants, Tyr96Ala and Tyr96Phe. When titrating M3-NTD Tyr96Ala into CLC peptide II-44, which bound to wild type M3-NTD with low micromolar K_D, no binding was observed (Figure 4E). The more conservative substitution of Tyr96 with Phe also severely reduced the affinity for II-44 (K_D = 100…300 µM) (Figure 4F), suggesting that the water-mediated interaction between Tyr96 and the peptide backbone strongly contributes to binding. This supports the critical role of Tyr96 in collagen binding, both via forming van der Waals interactions with the collagen peptide triple helix as well as forming the water-mediated polar interaction with the peptide backbone. In conclusion, we present the first structural evidence for an M-protein collagen complex. The structure indicates a general binding mechanism that might explain the promiscuity of M3 for diverse CLC peptides and explains how M3 is able to bind non-selectively to different collagens.

emm *type-dependent effect of human collagen on biofilm formation by GAS strains*

GAS *emm*3 strains are highly prevalent in necrotizing soft tissue infections [19, 20], where they have been found to form biofilm [18]. Based on our previous data demonstrating that the tissue milieu seems to promote GAS biofilm [18], and with collagen being a ubiquitous structural protein, it was of interest to assess whether the M3-collagen interaction could affect biofilm formation. For this purpose, we used crystal-violet based assay to determine biofilm formation by GAS strains from patients with necrotizing soft tissue infections on polystyrene plates, either uncoated or coated with

400 human type I collagen. The three isolates, *emm*1, *emm*3 and *emm*28 strains, all formed biofilm on
401 uncoated plates (Figure 9A). Notably, on collagen-coated plates, biofilm of isolates 2006 (*emm*1)
402 and 5004 (*emm*28) was significantly reduced in a dose-dependent manner, while that of isolate 2028
403 (*emm*3) was significantly enhanced (Figure 9B, C). The collagen-enhancing effect of biofilm for the
404 *emm*3 strain was seen even at inocula as low as 100 CFU/well (Figure 9D), where also a dose-
405 response to collagen was evident (Figure 9D). Confocal microscopy was used to assess bacterial
406 attachment and biofilm formation with bacteria grown on glass slides with or without collagen coating.
407 In line with the crystal-violet assay, bacterial attachment of the *emm*1 (2006) and the *emm*28 (5004)
408 strain was almost completely blocked by collagen whereas the *emm*3 (2028) strain formed strong
409 robust biofilm in the presence of collagen (Figure 9E).
410

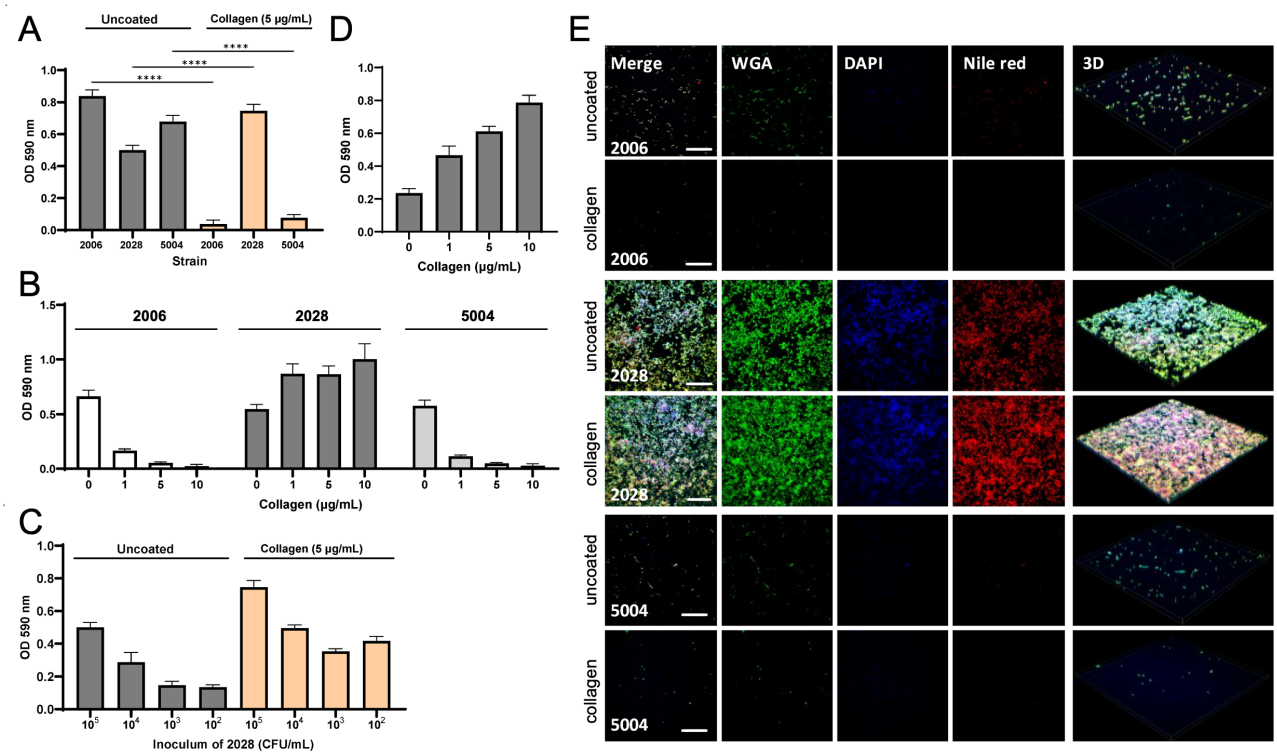

411
412 Figure 9. Effect of collagen type I on biofilm formation by necrotizing soft tissue infections strains. A)
413 Quantitative analysis of biofilm formation on polystyrene surface with or without human type I
414 collagen. The inoculum of each bacterial strain was 10^5 CFU per well. Significance was determined
415 by one-way ANOVA with Tukey's *post-hoc* test. ****, P<0.0001; ***, P< 0.001; **, P< 0.01; *, P< 0.05
416 B) Varying effect of collagen concentration. The inoculum of each bacterial strain was 10^5 CFU per
417 well. C) Inoculum effects on biofilm of strain 2028. D) Effect of concentration of coating collagen on
418 strain 2028 biofilm (100 CFU per well). A-D) Results are shown as Mean + SE. All assays were
419 repeated at least three times in triplicate. E) Confocal microscopic analysis of biofilm formation 48 h
420 after incubation. Fluorescence staining (WGA-Alexa 488, DAPI, and Nile red) of biofilm on uncoated
421 and collagen-coated glass slides. Scale bars indicate 50 µm.

422

423 Taken together the data shows a collagen-enhanced biofilm formation for the *emm*3, but not the
424 *emm*1 and *emm*28 strains. To test whether this effect was linked to the M3-protein/collagen
425 interaction, we performed competition experiments where biofilm formation of the *emm*3 (2028)
426 strain was assessed in the presence of increasing concentrations of M3-NTD in the medium. The
427 enhancing effect of collagen was almost completely negated in presence of 20 μM M3-NTD (Figure
428 10).

429

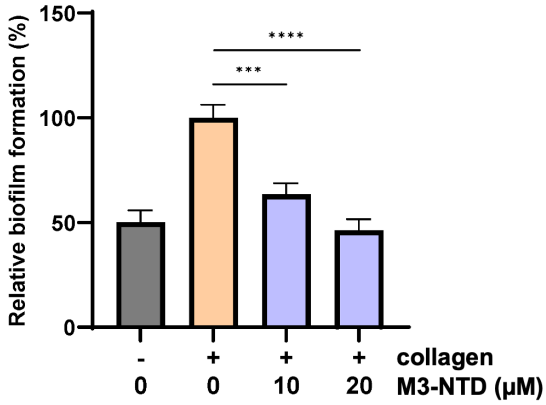

430

431 Figure 10. Competition analysis of biofilm formation of GAS isolate 2028 (100 CFU per well) in the
432 presence of M3-NTD. Results are shown as Mean + SE. All assays were repeated three times in
433 triplicate. Significance was determined by one-way ANOVA, followed by Tukey's *post-hoc* test ****,
434 P<0.0001; ***, P< 0.001.

435

436 These data indicate that the interaction between M3 protein and collagen enhances biofilm
437 formation. In further support of this finding, two additional *emm*3 strains, GAS 5626 and 8003 showed
438 a similar increase in biofilm formation on collagen-coated plates (Figure 10—figure supplement 1A).
439 The expression of M3 protein by all three *emm*3 strains was confirmed using an M3-specific antibody
440 (Figure 10—figure supplement 1B).

441

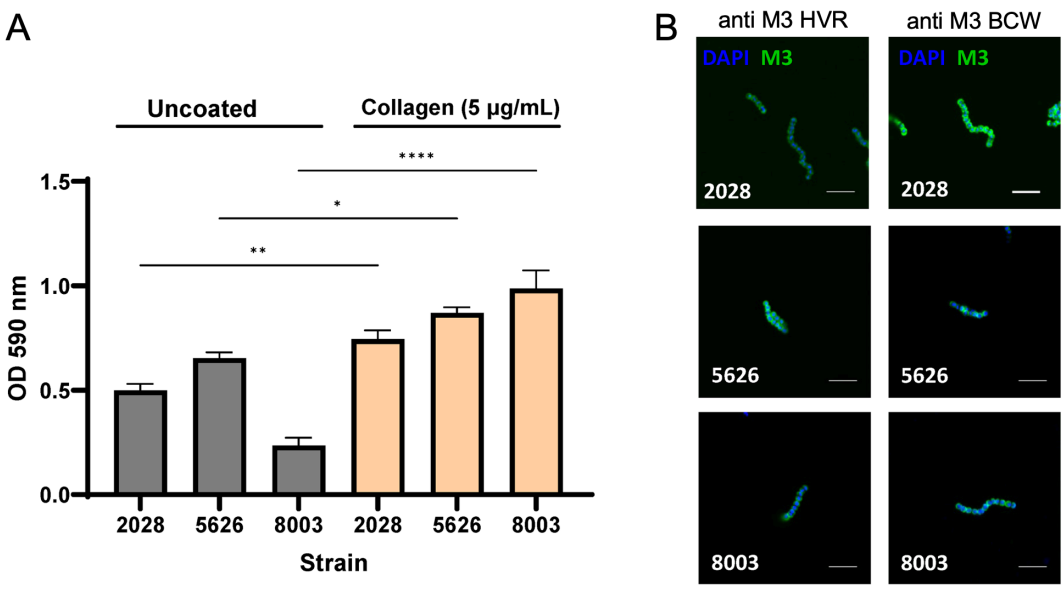

Figure 10—figure supplement 1. Biofilm formation of *emm*3 GAS. A) Quantitative analysis of biofilm formation on polystyrene surface with or without human type I collagen. The inoculum of each bacterial strain was 10^5 CFU per well. This assay was repeated at four times in triplicate and results are shown as Mean + SE. Significance was determined by one-way ANOVA with Tukey's *post-hoc* test. ****, P<0.0001; ***, P< 0.001; **, P< 0.01; *, P< 0.05. B) Confocal image of *emm*3 GAS stained with DAPI and M3-specific antibodies. BCW, B- and C-repeat and wall-spanning regions of M3. Scale bars indicate 5 µm.

GAS M3-collagen interaction in patient biopsies and in a 3D skin tissue model

To demonstrate a potential interaction between GAS and collagen during infection, we stained tissue biopsies from patients with necrotizing soft tissue infections using specific anti-GAS and anti-collagen IV antibodies (Figure 11). In areas with high bacterial load, collagen was observed to co-localize with the bacteria in biopsies from two patients infected with *emm*3 strains 2028 and 5020. In contrast, in patients infected with *emm*1strains (2006 and 2068), no co-localization between the bacteria and collagen was evident.

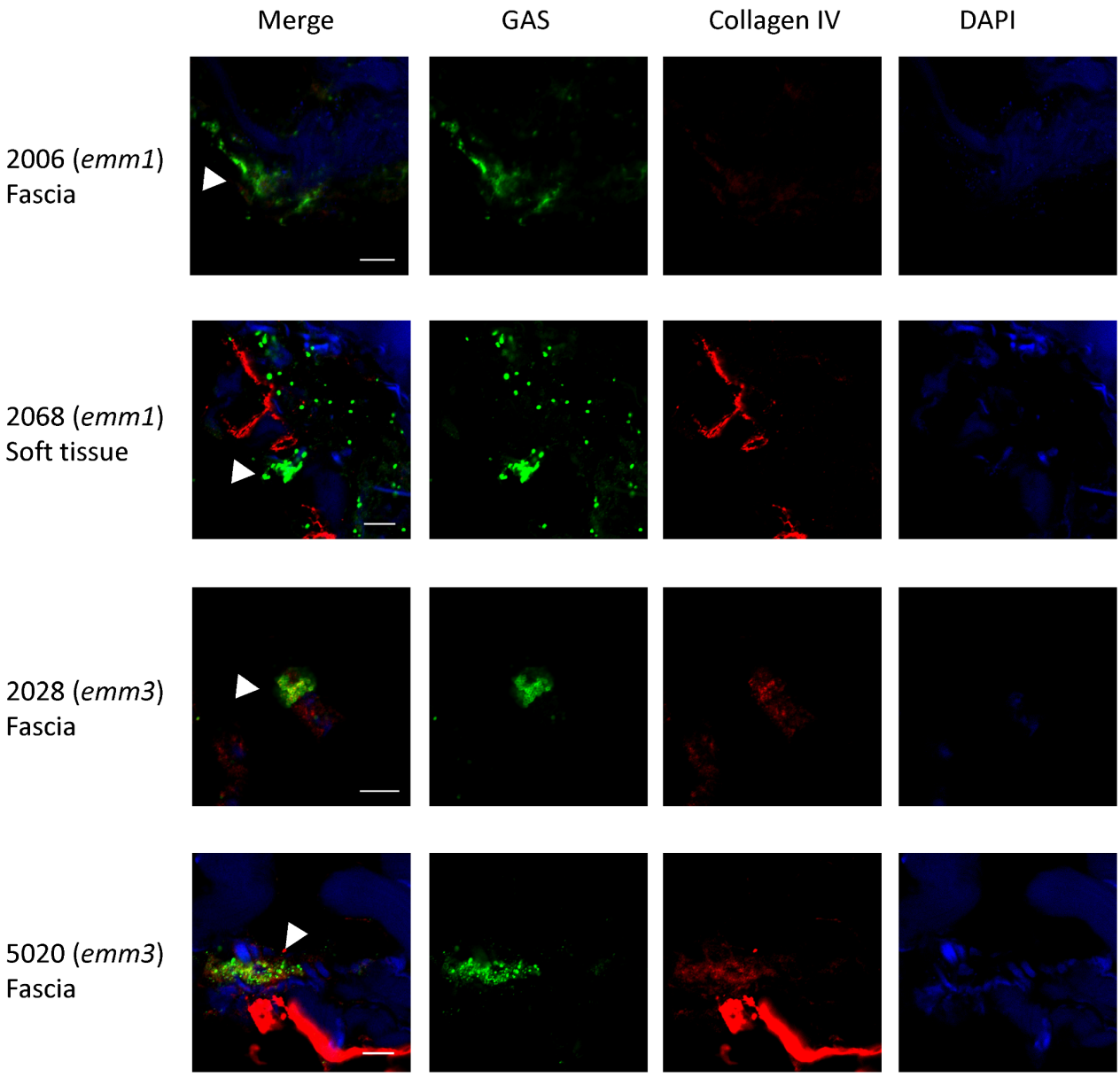

459

460 Figure 11. Colocalization of collagen with *emm3* GAS in patients' biopsies. Frozen biopsy sections
461 were stained with anti-GAS (green), anti-collagen IV (red) and DAPI (blue). Scale bars indicate 50
462 µm.

463

464 To further investigate this in a more controlled infection model, we used a human 3D organotypic
465 skin model, which is based on a collagen type IV scaffold. We have previously employed this tissue
466 model for studies of biofilm and GAS-elicited tissue pathology [51, 52]. Infection of the skin
467 organotypic tissue with the *emm*1 (2006) and *emm*3 (2028) strains showed that both strains
468 efficiently infected the skin model tissue and caused disruption of the epithelial layer (Figure 12).
469 Bacterial load and tissue pathology increased over time. Collagen began to colocalize with *emm*3
470 GAS 8 h after infection and strongly colocalized with bacteria 24 and 48 h after infection. In contrast,
471 no colocalization of collagen and *emm*1 GAS was observed. These data suggest that an interaction

472 between *emm*3 GAS and collagen occurs in human tissue and might be an important factor for
473 biofilm formation.
474

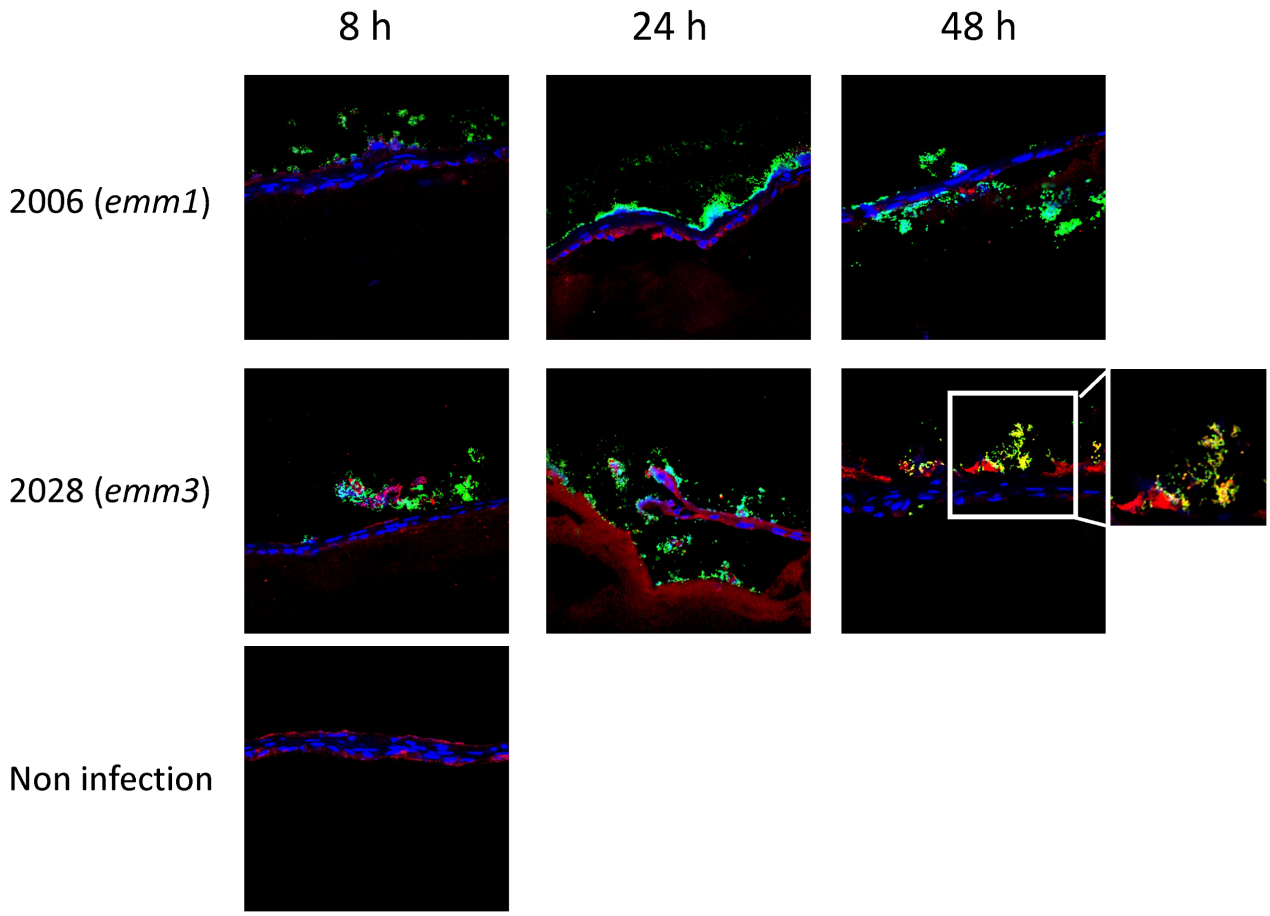

475
476 Figure 12. Colocalization of collagen with *emm3* GAS in 3D skin tissue model. Skin tissue models
477 were infected with GAS strains 2006 and 2028. At 8, 24 and 48 hours after infection, frozen sections
478 were stained with anti-GAS (green), anti-collagen IV (red) and DAPI (blue). The merged images are
479 shown.
480
481
482 **Discussion**
483
484 No obvious or simple connection can be made between M protein sequences and the differential
485 abilities of the over 200 variants to interact with host factors. At least some activities of this major
486 streptococcal virulence factor may be encoded in hidden sequence patterns, as identified for the M4-
487 binding protein interaction with HVRs [14]. In this study, we show that the HVR of the M3 protein
488 deviates from the canonical coiled-coil structure generally assumed to be adopted by M proteins.
489 The novel T-shaped fold identified here is required for the collagen binding activity of M3. While this
490 fold may be limited to a few phylogenetically close variants of M proteins in GAS, it is more abundant

491 in SDSE. The discovery of a folded HVR may inform vaccine design. Although immunization with
492 short and therefore monomeric M protein HVR peptides may be sufficient for most GAS serotypes,
493 immunogenic epitopes of M3 may only be present in the folded, dimeric form of the protein.
494 The structures of M3-NTD alone and in presence of a collagen peptide give a rational basis for the
495 role of the PARF motif, which was previously implicated in collagen binding [33]. The role of
496 conserved residues within PARF is predominantly to stabilize the T-fold of M3-NTD. The motif alone,
497 encompassing eight residues (Ala94 to Asn101) as defined by Barroso *et al.* [32], does not present
498 all structural features involved in collagen binding based on our structure. This depends on a larger
499 region spanning residues Gln92 to Leu107 on the H2 helix, with some minor contributions of residues
500 in H1 (Figure 8). The complex structure identifies Tyr96 and Trp103 as key interface residues. They
501 provide shape complementarity and stack against proline and hydroxyproline rings of the collagen
502 triple helix. Our mutational analysis confirms a role in collagen binding for Tyr96. Conclusions from
503 the crystal structure are consistent with our analysis of the binding propensities of the different amino
504 acids in the CLC peptides. The observed prominent roles for hydrophobic residues and for
505 hydroxyproline in the solid-phase binding assays would be predicted from the complex structure.
506 The negative effects on binding rank of glutamate and of proline are less easy to explain. Proline is
507 restricted to the X position of the GXY triplet, which is also the position usually occupied by
508 glutamate. The effect of both residues may be to exclude more productive hydrophobic amino acids
509 from the X position. The positive role of hydroxyproline in the Y position is amply demonstrated in
510 the crystal structure. In addition to its ability to form hydrogen bonds, this may derive from its greater
511 extension from the helix axis than proline. Our findings are reminiscent of those obtained for YadA
512 [39], in that we also observed promiscuous binding to the CLC peptides, which was strongly
513 dependent on hydrophobic residues. However, in the case of YadA, the number of GPO triplets and
514 number of both Pro and Hyp also correlated with affinity.
515 The molecular complex described here explains how GAS of the M3 type achieve very strong binding
516 to collagens. While the affinity for the triple helical peptides measured here by ITC is moderate, the
517 presence of two binding sites on the HVR that is found at the distal end of each M3 protein suggests
518 cooperative binding in the context of larger collagen assemblies. Most likely the bacteria do not
519 encounter isolated triple-helices, but higher-order collagen structures made of bundles of triple
520 helices. It can be envisaged how M3 proteins probably intercalate between triple helices in such
521 higher-order assemblies. Given the high density of M proteins on GAS surfaces, this would generate
522 a highly polyvalent host-bacteria interface with the HVR acting as an anchor binding M3
523 perpendicularly to collagen fibrils/fibers. It is also at this higher-order structural level that an
524 explanation for the ability of M3 to induce an anti-collagen autoimmune response might be found. In
525 the rare autoimmune disease Goodpasture syndrome, an anti-collagen response is thought to be
526 caused by collagen IV neoepitopes, with infections being suggested as one possible cause for their
527 exposure [53]. It is conceivable that such neoepitopes could be generated as a result of collagen

528 structural changes caused by M3 protein binding. However, such structural rearrangements could
529 not be observed in our simplified molecular system, and our data cannot provide evidence backing
530 the anti-collagen hypothesis of post-streptococcal rheumatic sequelae [41] beyond providing the
531 molecular basis for collagen recognition by M3 protein.
532 The structural data presented here allow us to conclude that collagen binding by M proteins relies
533 on the presence of a T-shaped helical bundle domain combined with key residues to provide shape
534 complementarity to tropocollagen triple helices. But even if all GAS M protein variants included in
535 our sequence analysis bound collagens in a similar manner to M3, this would still indicate that M3-
536 like collagen binding mechanism is rare among GAS M protein variants. Based on data published
537 for M55, which was found to bind comparably weakly to collagen IV [54], it seems likely that M3 and
538 closely related serotypes have a unique ability to bind collagens in the way described here.
539 AlphaFold3 predictions support this, yielding converging structural models for the M3-collagen
540 peptide complex that closely resembled our experimental structure. This was also true for M31 and
541 M222. However, predictions with M12 and M55 resulted in low-confidence, non-converging structural
542 models with poorly defined binding sites, and/or disruption of the T-fold (Figure 6—figure supplement
543 1). On the other hand, highly confident structural predictions together with conservation of key
544 residues suggests the M3-like collagen binding mechanism is shared by SDSE and SESZ M proteins
545 (Figure 6—figure supplement 1). This has previously been experimentally validated for the FOG (or
546 Stg11) protein of SDSE, which was found to bind to collagens I and IV with high affinity [33, 42].
547 SDSE, in the past often associated with animal infections, is increasingly recognized as a highly
548 prevalent human pathogen closely resembling GAS in terms of virulence traits and pathologies,
549 including invasive infections, post-infection autoimmune sequelae [35] and biofilm formation [55].
550 Collagen binding by M proteins may be therefore a far more common virulence mechanism in human
551 streptococcal infections than the prevalence of *emm*3 GAS alone would suggest. It should be noted,
552 too, that a new *emm*3 variant, *emm*3.93, is currently emerging in the UK and the Netherlands, with
553 a high prevalence in invasive infections [56].
554 The interaction between M protein and collagen has implications for several biological functions,
555 including bacterial attachment and biofilm formation. In this study, we investigated biofilm formation
556 due to the high prevalence of *emm*3 strains in necrotizing soft tissue infections [20], in which biofilm
557 is complicating feature [18, 57]. Our findings reveal that the M3 protein-collagen interaction promotes
558 biofilm in *emm*3 strains. Notably, for other *emm* types the presence of collagen appears to have an
559 opposing effect, reducing bacterial attachment and biofilm *in vitro* for other *emm* types. This type-
560 specific difference is further supported by observations within infected tissue where *emm*3 but not
561 *emm*1 strains co-localize with collagen fibers. These findings highlight the importance of collagen
562 for *emm*3 biofilm development in the tissue setting, while other GAS *emm* types likely utilize other
563 mechanisms. Further studies are warranted to explore the underlying mechanisms of biofilm
564 formation in streptococcal tissue infections, including not only GAS but also SDSE strains.

565 **Materials and Methods**

566

567 ***Cloning and site-directed mutagenesis***

568 M3-NTD DNA insert was amplified from a plasmid containing full M3 DNA sequence using primers
569 5'-GCTAGCCATGGATGCTAGGAGTGTTAATGG-3' and 5'-
570 CTAGGGATCCCTAGCAGTCCTGATATTCCTTTTC-3', digested with NcoI and BamHI and ligated
571 into the pEHISTEV vector [58], pre-digested with the same enzymes. The final M3-NTD construct,
572 after digestion with TEV protease, comprised 113 amino acids starting with Gly-Ala-Met, an artefact
573 of the purification tag. Site-directed mutagenesis was performed by PCR amplification of pEHISTEV-
574 M3NTD plasmid using mutagenic primers listed in Table 3. For selenomethionine labelling, two
575 methionine residues were introduced by substituting Ile60 and Ile141 using two sequential rounds
576 of site-directed mutagenesis.

577

578 Table 3. List of mutagenic primers.

MUTATION	PRIMER SEQUENCE (5'→3')
Tyr96Ala	GACAAAAGGCTGAAGCGCTAAAAGGCC
	GGCCTTTTAGCGCTTCAGCCTTTTGTC
Tyr96Gln	GACAAAAGGCTGAACAACTAAAAGGCC
	GGCCTTTTAGTTGTTCAGCCTTTTGTC
Tyr96Phe	GACAAAAGGCTGAATTTCTAAAAGGCC
	GGCCTTTTAGAAATTCAGCCTTTTGTC
Ile60Met	GTTAAATTAAAAAATGAAATGGAGAACTTGTTAGATC
	GATCTAACAAGTTCTCCATTTCATTTTTTAATTTAAC
Ile141Met	GAACTTAAGGAAAAAATGGACAAAAAGGAAAAGG
	CCTTTTCCTTTTTGTCCATTTTTTCCTTAAGTTC

579

580 ***Recombinant protein production***

581 Recombinant M3 protein was produced as an GST fusion construct as previously described [59]
582 from a pGEX6P-1 vector, a kind gift from Dr Susanne Talay, in *E. coli* BL21 (DE3) cells. The cells
583 were grown in LB media containing 100 mg mL^{-1} ampicillin at 37 ºC for 3 h after growth to an optical
584 density at 600 nm of 0.6, and induction with 1 mM isopropyl β-D-1-thiogalactopyranoside. The fusion
585 protein was purified from bacterial cell lysate using a GSTrap 4B column according to the protocol
586 provided by the manufacturer (Cytiva). The recombinant protein comprised GST fused to a
587 proteolytic cleavage site (not used in this study) and the N-terminus of M3 (UniProt entry
588 A0A0H2UWN1), lacking N-terminal secretion signal, cell wall anchor and membrane spanning
589 region (residues 42-546).

590 M3-NTD constructs were overexpressed from pEHISTEV plasmid in *E. coli* soluBL21 cells
591 (Genlantis), in a standard LB medium supplemented with 50 mg mL^{-1} kanamycin. An overnight
592 culture was used to inoculate flasks containing 1 L of the growth medium which were incubated at
593 37 ºC with shaking. When the optical density at 600nm was 0.5-0.8 expression was induced by
594 adding IPTG to a final concentration of 1mM. After 3-4 h of further incubation with shaking the cells
595 were harvested and frozen. For selenomethionine labelling the pHT-M3-NTD [Ile60Met, Ile141Met]
596 plasmid was introduced into the methionine auxotroph strain of *E. coli*, B834, which was obtained
597 from Dr Clarissa Melo Czekster. The cells from the overnight culture were washed twice with M9
598 minimal media, resuspended in 0.2x the initial volume and used to inoculate (10 mL per L) of
599 SelenoMet medium (Molecular Dimensions) supplemented with 0.04 mg L^{-1} L-selenomethionine
600 (ThermoFisher). Following induction of expression, the cells were incubated with shaking for 5 h.
601 Cell pellets were resuspended in 50-100 mL 50 mM Tris-HCl pH 8, 500 mM NaCl lysis buffer
602 supplemented with one cOmplete protease inhibitor tablet (Roche) and 1 mg DNAse I (Merck). The
603 suspension was passed twice through a Cell Disrupter (Constant Systems) at 30 kpsi and the lysate
604 was clarified by centrifugation at 20,000 x g for 25 min at 4 ºC. The supernatant was applied to a
605 HisTrap column (Cytiva) pre-equilibrated in the lysis buffer and the bound protein was washed with
606 10 column volumes of the wash buffer (50 mM Tris-HCl pH 8, 500 mM NaCl, 20 mM imidazole) and
607 eluted in a linear gradient (20-250 mM imidazole). To remove imidazole and the N-terminal
608 purification tag, the eluate was mixed with TEV protease (produced in-house) at approximately 30:1
609 stoichiometric ratio and dialyzed overnight at room temperature against PBS supplemented with 1
610 mM DTT. The digested protein solution was passed through the HisTrap column again, with PBS as
611 the mobile phase, and M3-NTD collected in the flow-through. Following concentration in 10 kDa
612 Amicon Ultra centrifugal filters (Millipore) the protein was further purified by size exclusion
613 chromatography using Superdex75 10/300 column (Cytiva) pre-equilibrated in PBS. Purity and
614 oxidation state were verified by SDS-PAGE. If some monomeric protein was still evident on the gel
615 the fractions from size exclusion chromatography were left overnight at 4 ºC. Fully oxidised protein
616 was concentrated, aliquoted and flash frozen.
617
618 ***Collagen peptides***
619 The Collagen Ligand Collection (CLC) peptides (formerly known as Collagen Toolkits) were obtained
620 as C-terminal amides from Triple Helical Peptides Ltd, Cambridge, UK. They were synthesised on
621 TentaGel R-Ram resin using Fmoc/tBu chemistry, either on an Applied Biosystems Pioneer peptide
622 synthesiser as described previously [60], or a CEM Liberty or Liberty Blue microwave-assisted
623 peptide synthesiser. Fractions containing homogeneous product were identified by analytical HPLC
624 on an ACEphenyl300 (5 mm) column, characterised by MALDI-TOF mass spectrometry, pooled and
625 freeze-dried. In the CLCs, the variable 27-residue primary collagen structure (guest sequence) was

626 flanked by GPC[GPP]$_5$- and -[GPP]$_5$GPC (host) peptides, to ensure stable triple-helical form. In
627 JDM238, the guest sequence is GVOGEA and the host sequences [GPO]$_3$.
628
629 ***Solid phase CLC binding assay***
630 CLC peptide solid-phase binding assays were performed following a previously published protocol
631 [45, 47]. Briefly, CLC peptides, collagen II (positive control), GPP10 and BSA (negative controls) (10
632 µg/ml in 0.01 M acetic acid) were immobilized on Immulon2 HB 96-well plates (Nunc, Langenselbold,
633 Germany) overnight at 4 ºC. All subsequent incubation steps were for 1 h at 25 ºC. The assay volume
634 was 100 µl per well. Wells were washed three times with adhesion buffer (0.1% (v/v) Tween-20 and
635 1 mg/ml BSA in PBS) between incubation steps. The wells were blocked with 50 mg/ml BSA in PBS
636 prior to the addition of recombinant GST-M3 at a concentration of 10 µg/ml in adhesion buffer. Bound
637 protein was detected with biotin goat anti-GST antibody (Abcam) at a 1:500 dilution in adhesion
638 buffer, followed by streptavidin-fused HRP and 3,3',5,5'-tetramethylbenzidine liquid substrate
639 system (Sigma), and plates read at 450 nm. Including Tween in the washing steps reduced
640 background signal but did not change the overall outcome for CLC-II. It was omitted for the CLC-III
641 assay.
642
643 ***NMR***
644 M3-NTD was isotopically labeled by expression in M9 minimal media (6.8 g/L Na_2HPO_4, 3.0 g/L
645 KH_2PO_4, 0.5 g/L NaCl, 1.0 g/L $^{15}NH_4Cl$, 2 mM $MgSO_4$, 0.1 mM $CaCl_2$, 1% (w/v) glucose, 1 mM
646 $MgSO_4$, 2.125 g/L BDTM Difco™ Yeast Nitrogen Base without Amino Acids and Ammonium Sulfate
647 (Thermo Fisher) and 50µg/ml kanamycin) and purified as described above for unlabeled protein.
648 The NMR sample contained 0.4 mM protein in 10 mM phosphate, 50 mM NaCl, pH 6.5, 1.5% (v/v)
649 D_2O, without or with addition of 10 mM DTT to generate monomeric M3-NTD. ^1H,^{15}N HSQC spectra
650 were recorded on a Bruker Ascend 700 MHz spectrometer equipped with a Prodigy TCI probe and
651 controlled by Bruker Topspin 3 software at 30 ºC. A standard Bruker pulse sequence with gradients
652 and water flip back pulse (hsqcetfpf3gpsi) was used with 20 transients and spectral resolutions or
653 14.5 Hz and 41.2 Hz in the direct (^1H) and indirect (^{15}N) dimension, respectively. Spectra were
654 processed with NMRPipe [61] and visualized with CCPN Analysis 2 [62].
655
656 ***Isothermal titration calorimetry***
657 The experiments were performed using MicroCal PEAQ-ITC instrument (Malvern Panalytical) at 25
658 ºC in PBS, with the reference power set to 3 µcal/s and stirring speed to 750 rpm. The cell contained
659 the CLC peptide at 40-90 µM (trimer), reconstituted in PBS, and the injector syringe contained M3-
660 NTD at 0.9-1.1 mM, dialysed in the same buffer. For control experiments determining the heats of
661 dilution, the cell contained PBS buffer only. Titration involved injection volumes of 2 µl except for the
662 first injection of 0.4 µl.

663

664 ***Protein crystallisation and structure determination***

665 Crystallization trials were conducted using the vapor diffusion sitting drop method and several sparse
666 matrix screens. M3-NTD protein construct was freshly purified by size-exclusion chromatography
667 and concentrated to ~700 µM. For co-crystallization with JDM238 peptide, the protein was
668 concentrated to 1 mM and then diluted by adding reconstituted peptide so that the final concentration
669 of M3-NTD was ~700 µM with triple-helical peptide at ~1.1 mM (1:1.5 ratio). The crystals of M3-NTD
670 grew at 20 ºC within 1-2 weeks in 40-50% MPD, and the best one diffracted to 1.92 Å resolution.
671 They were used for streak-seeding the selenomethionine-labelled protein, which resulted in shard-
672 like crystals diffracting to 2.67 Å with the data collected at the selenium K absorption edge. Phasing
673 of the SAD dataset was conducted automatically by the Diamond Light Source (DLS) pipeline
674 FastEP and initial model building was performed using the ARP/wARP software package. The
675 crystals of M3-NTD in complex with the collagen peptide were obtained in 15% PEG 10K, 0.1 M
676 Tris-HCl pH 8.5, 0.29 M $MgSO_4$ and diffracted to 2.32 Å resolution. Indexing, scaling and merging of
677 data was performed using the autoPROC pipeline at the DLS. The complex structure was solved by
678 molecular replacement with PHASER [63] using M3-NTD and collagen peptide (PDB 3P46)
679 structures and as search models, with all non-proline residues in the collagen peptide model
680 substituted with alanine. For both structures, iterative model building and refinement was performed
681 using Coot [64] and Refmac5 [65]. MolProbity [66] was used for model quality assessment. Figures
682 of protein structure models were produced using PyMOL (Schrödinger, LLC).

683

684 ***Accession codes***

685 The M3-NTD and M3-NTD/JDM238 protein structures and the data used to derive these, have been
686 deposited at the PDBe with accession codes 8p6k and 8p6j, respectively.

687

688 ***Bacterial strains***

689 GAS strains 2006 (*emm1*), 2028 (*emm3*), and 5004 (*emm28*) are isolates from patients with
690 necrotizing soft tissue infections from the INFECT project [18]. GAS 5262 and 8003 were provided
691 by Donald E. Low (Mount Sinai Hospital, Toronto, Canada) and used as further *emm3* isolates from
692 patients with necrotizing soft tissue infections [67, 68]. All isolates were cultured in either Todd-Hewitt
693 broth supplemented with 1.5% yeast extract or brain heart infusion broth at 37 ºC under a 5% CO_2
694 atmosphere.

695

696 ***Biofilm formation assay on a polystyrene surface***

697 Biofilm formation was evaluated by crystal violet staining as described previously, with minor
698 modifications [69]. Overnight cultures of the bacteria being tested were washed with PBS and diluted
699 to approximately 10^6 CFU/mL. Bacterial suspensions (100 µL) were seeded into 96-well polystyrene

700 plates (Thermo Fisher Scientific, Waltham, MA, USA). The plates were then incubated for 24 h at 37
701 ºC. After incubation, planktonic bacteria were removed by washing with PBS. Plates were then
702 stained with a 0.1% crystal violet solution (Invitrogen, Waltham, MA, USA) for 30 min. Excess crystal
703 violet was removed by washing with PBS, and then the crystal violet that was associated with
704 bacterial cells was eluted with absolute ethanol. The amount of crystal violet (and by association,
705 biofilm) was evaluated by measuring the absorbance at 590 nm using a spectrophotometer.
706 Collagen-coated plates were prepared by incubating plates with 1-10 µg/mL of collagen I overnight
707 at 4 ºC.
708
709 ***Confocal microscopic analysis of biofilm formation***
710 The biofilms were formed on an 8-well chamber slide (Lab-Tek, Thermo Fisher Scientific) in the
711 same manner as for the biofilm assay. After removing planktonic bacteria by washing with PBS, the
712 biofilms were fixed with 10% formalin and stained with wheat germ agglutinin (WGA)-Alexa Fluor
713 488 conjugate (Invitrogen) and Nile red (Invitrogen). The slides were mounted using ProLong™ Gold
714 Antifade Mountant with DAPI (Invitrogen).
715
716 ***Biofilm competition assay***
717 Recombinant M3-NTD was added at 10 and 20 µM concentrations in PBS to a collagen-coated 96-
718 well plate (0.5 µg/well) and the plate was incubated for 1 h at room temperature. After removal of
719 the protein solution, 100 µL of strain 2028 culture (ca. 10^3 CFU/mL) was seeded and incubated for
720 24 h. Biofilms were stained with crystal violet, as described above.
721
722 ***Immunofluorescent staining of GAS***
723 A few colonies were suspended in PBS on a glass slide and then fixed in 3.7% formaldehyde in PBS
724 for 15 min. The bacteria were stained with anti-M3 specific antibodies (kindly provided by Prof.
725 Gunnar Lindahl, Lund University), followed by WGA-Alexa Fluor 488 conjugate antibodies
726 (Invitrogen). The slides were mounted using ProLong™ Gold Antifade Mountant with DAPI
727 (Invitrogen).
728
729 ***Three-dimensional organotypic skin model***
730 The 3D skin models were constructed as described previously [18, 51, 52]. Briefly, 4.0×10^4 normal
731 human dermal fibroblasts (NHDF) in a collagen matrix (Pure Col, Advanced Biomatrix, Carlsbad,
732 CA, USA) were seeded onto a polymerized cell-free collagen layer in a 6-well filter insert (Corning,
733 Corning, NY, USA). After culturing in DMEM for one week, 1.0×10^6 human keratinocyte cells
734 N/TERT-1 were seeded onto the NHDF layer. The models were cultured in EpiLife medium
735 (Invitrogen) for three days and exposed to air for one week. For the infection assay, the models were
736 infected with 1×10^6 CFU of bacteria for 8, 24, or 48 h.

737

738 ***Immunofluorescent staining of patient tissue biopsies and tissue models***

739 Snapfrozen tissue biopsies from patients with necrotizing soft tissue infections caused by either
740 *emm1* GAS strains *(*patients 2006 and 2068) or *emm*3 GAS (patients 2028 and 5020) were available
741 from the INFECT patient biobank [18]. Cryosectioning and staining were performed as previously
742 described [52]. Briefly, the biopsies and models were embedded in an optimum cutting temperature
743 compound (Sakura, Torrance, CA, USA) and frozen in liquid nitrogen. Cryosectioning (8 µm) was
744 performed using a Leica CM3050 cryostat (Leica, Nußloch, Germany). Sections were then fixed in
745 3.7% formaldehyde in PBS for 15 min and stained with both anti-GAS (goat polyclonal antibody,
746 Abcam, Cambridge, UK) and anti-collagen IV antibodies (Abcam, Cambridge, UK), followed by
747 WGA-Alexa Fluor 488 and 546 conjugate antibodies (Invitrogen).

748

749 ***Statistical Analysis***

750 To compare the propensity of specific CLC amino acids to contribute to M3 binding, the A_{450} value
751 for M3 binding to BSA was subtracted from all values obtained from the solid-phase binding assays.
752 This allowed the CLC peptides to be ranked in descending order of A_{450} and divided into three
753 absorbance groups: high, from 0.75 to 0.5; medium, from 0.5 to 0.25; and low, from 0.25 to zero.
754 Data from both CLCs were pooled, and the amino acid abundance in the three groups was
755 compared. For each peptide from CLC-II and CLC-III, the number of occurrences of each amino acid
756 of interest was noted. The non-parametric Kruskal-Wallis test was used to determine whether the
757 amino acid abundance differed between the three groups. For the biofilm experiments, One-way
758 ANOVA with the Tukey's *post-hoc* test was used to determine statistically significant differences.

759

760

761 **References**

762

763 1. Brouwer S, Rivera-Hernandez T, Curren BF, Harbison-Price N, De Oliveira DMP, Jespersen
764 MG, Davies MR, Walker MJ. Pathogenesis, epidemiology and control of Group A Streptococcus
765 infection (2023) *Nature Reviews Microbiology* **21**:431-447 10.1038/s41579-023-00865-7.

766 2. Carapetis JR, Steer AC, Mulholland EK, Weber M. The global burden of group A streptococcal
767 diseases (2005) *The Lancet Infectious Diseases* **5**:685-94

768 3. Jackson SJ, Steer AC, Campbell H. Systematic Review: Estimation of global burden of non-
769 suppurative sequelae of upper respiratory tract infection: rheumatic fever and post-streptococcal
770 glomerulonephritis (2011) *Tropical Medicine & International Health* **16**:2-11 10.1111/j.1365-
771 3156.2010.02670.x.

772 4. Bagcchi S. Surge of invasive Group A Streptococcus disease (2023) *Lancet Infectious Diseases*
773 **23**:284-284 10.1016/s1473-3099(23)00043-9.

774 5. Oehmcke S, Shannon O, Morgelin M, Herwald H. Streptococcal M proteins and their role as
775 virulence determinants (2010) *Clinica Chimica Acta; International Journal of Clinical Chemistry*
776 **411**:1172-80 10.1016/j.cca.2010.04.032.

6. Smeesters PR, McMillan DJ, Sriprakash KS. The streptococcal M protein: a highly versatile molecule (2010) *Trends in Microbiology* **18**:275-282 10.1016/j.tim.2010.02.007.

7. Walker MJ, Barnett TC, McArthur JD, Cole JN, Gillen CM, Henningham A, Sriprakash KS, Sanderson-Smith ML, Nizet V. Disease manifestations and pathogenic mechanisms of Group A Streptococcus (2014) *Clinical Microbiology Reviews* **27**:264-301 10.1128/CMR.00101-13.

8. Phillips GN, Jr., Flicker PF, Cohen C, Manjula BN, Fischetti VA. Streptococcal M protein: alpha-helical coiled-coil structure and arrangement on the cell surface (1981) *Proceedings of the National Academy of Sciences of the United States of America* **78**:4689-93

9. Nilson BHK, Frick IM, Akesson P, Forsen S, Bjorck L, Akerstrom B, Wikstrom M. Structure and stability of protein-H and the M1 protein from Streptococcus-pyogenes - implications for other surface-proteins of Gram-positive bacteria (1995) *Biochemistry* **34**:13688-13698 10.1021/bi00041a051.

10. Sanderson-Smith M, De Oliveira DMP, Guglielmini J, McMillan DJ, Vu T, Holien JK, Henningham A, Steer AC [...], Grp MPS. A Systematic and Functional Classification of *Streptococcus pyogenes* That Serves as a New Tool for Molecular Typing and Vaccine Development (2014) *Journal of Infectious Diseases* **210**:1325-1338 10.1093/infdis/jiu260.

11. Macheboeuf P, Buffalo C, Fu CY, Zinkernagel AS, Cole JN, Johnson JE, Nizet V, Ghosh P. Streptococcal M1 protein constructs a pathological host fibrinogen network (2011) *Nature* **472**:64-8 10.1038/nature09967.

12. McNamara C, Zinkernagel AS, Macheboeuf P, Cunningham MW, Nizet V, Ghosh P. Coiled-coil irregularities and instabilities in group A Streptococcus M1 are required for virulence (2008) *Science* **319**:1405-8

13. Stewart CM, Buffalo CZ, Valderrama JA, Henningham A, Cole JN, Nizet V, Ghosh P. Coiled-coil destabilizing residues in the group A Streptococcus M1 protein are required for functional interaction (2016) *Proceedings of the National Academy of Sciences of the United States of America* **113**:9515-9520 10.1073/pnas.1606160113.

14. Buffalo CZ, Bahn-Suh AJ, Hirakis SP, Biswas T, Amaro RE, Nizet V, Ghosh P. Conserved patterns hidden within group A Streptococcus M protein hypervariability recognize human C4b-binding protein (2016) *Nature Microbiology* **1** 10.1038/nmicrobiol.2016.155.

15. Fiedler T, Koller T, Kreikemeyer B. *Streptococcus pyogenes* biofilms-formation, biology, and clinical relevance (2015) *Frontiers in Cellular and Infection Microbiology* **5**:15 10.3389/fcimb.2015.00015.

16. Hoiby N, Bjarnsholt T, Moser C, Bassi GL, Coenye T, Donelli G, Hall-Stoodley L, Hola V [...], Consulting External Expert Werner Z. ESCMID guideline for the diagnosis and treatment of biofilm infections 2014 (2015) *Clinical Microbiology and Infection* **21 Suppl 1**:S1-25 10.1016/j.cmi.2014.10.024.

17. Ciofu O, Moser C, Jensen PO, Hoiby N. Tolerance and resistance of microbial biofilms (2022) *Nature Reviews Microbiology* **20**:621-635 10.1038/s41579-022-00682-4.

18. Siemens N, Chakrakodi B, Shambat SM, Morgan M, Bergsten H, Hyldegaard O, Skrede S, Arnell P [...], Norrby-Teglund A. Biofilm in group A streptococcal necrotizing soft tissue infections (2016) *JCI Insight* **1**:e87882 10.1172/jci.insight.87882.

19. Luca-Harari B, Darenberg J, Neal S, Siljander T, Strakova L, Tanna A, Creti R, Ekelund K [...], Jasir A. Clinical and microbiological characteristics of severe *Streptococcus pyogenes* disease in Europe (2009) *Journal of Clinical Microbiology* **47**:1155-65 10.1128/JCM.02155-08.

20. Bruun T, Rath E, Madsen MB, Oppegaard O, Nekludov M, Arnell P, Karlsson Y, Babbar A [...], Group IS. Risk Factors and Predictors of Mortality in Streptococcal Necrotizing Soft-tissue Infections: A Multicenter Prospective Study (2021) *Clinical Infectious Diseases* **72**:293-300 10.1093/cid/ciaa027.

825 21. Lembke C, Podbielski A, Hidalgo-Grass C, Jonas L, Hanski E, Kreikemeyer B. Characterization
826 of biofilm formation by clinically relevant serotypes of group A streptococci (2006) *Applied and*
827 *Environmental Microbiology* **72**:2864-75 10.1128/AEM.72.4.2864-2875.2006.

828 22. Koller T, Manetti AGO, Kreikemeyer B, Lembke C, Margarit I, Grandi G, Podbielski A. Typing of
829 the pilus-protein-encoding FCT region and biofilm formation as novel parameters in
830 epidemiological investigations of *Streptococcus pyogenes* isolates from various infection sites
831 (2010) *Journal of Medical Microbiology* **59**:442-452 10.1099/jmm.0.013581-0.

832 23. Herwald H, Cramer H, Mörgelin M, Russell W, Sollenberg U, Norrby-Teglund A, Flodgaard H,
833 Lindbom L, Björck L. M protein, a classical bacterial virulence determinant, forms complexes
834 with fibrinogen that induce vascular leakage (2004) *Cell* **116**:367-379 Doi 10.1016/S0092-
835 8674(04)00057-1.

836 24. Thern A, Stenberg L, Dahlback B, Lindahl G. Ig-Binding Surface-Proteins of Streptococcus-
837 Pyogenes Also Bind Human C4b-Binding Protein (C4bp), a Regulatory Component of the
838 Complement-System (1995) *Journal of Immunology* **154**:375-386

839 25. Sanderson-Smith M, Batzloff M, Sriprakash KS, Dowton M, Ranson M, Walker MJ. Divergence
840 in the plasminogen-binding group A streptococcal M protein family - Functional conservation of
841 binding site and potential role for immune selection of variants (2006) *Journal of Biological*
842 *Chemistry* **281**:3217-3226 10.1074/jbc.M508758200.

843 26. Cue D, Lam H, Cleary PP. Genetic dissection of the M1 protein: regions involved in fibronectin
844 binding and intracellular invasion (2001) *Microbial Pathogenesis* **31**:231-242 DOI
845 10.1006/mpat.2001.0467.

846 27. Dinkla K, Rohde M, Jansen WT, Kaplan EL, Chhatwal GS, Talay SR. Rheumatic fever-
847 associated *Streptococcus pyogenes* isolates aggregate collagen (2003) *Journal of Clinical*
848 *Investigation* **111**:1905-12

849 28. Bessen DE. Localization of Immunoglobulin A-Binding Sites within M or M-Like Proteins of
850 Group-A Streptococci (1994) *Infection and Immunity* **62**:1968-1974 Doi 10.1128/Iai.62.5.1968-
851 1974.1994.

852 29. Quek AJH, Mazzitelli BA, Wu G, Leung EWW, Caradoc-Davies TT, Lloyd GJ, Jeevarajah D,
853 Conroy PJ [...], Law RHP. Structure and Function Characterization of the a1a2 Motifs of
854 *Streptococcus pyogenes* M Protein in Human Plasminogen Binding (2019) *Journal of Molecular*
855 *Biology* **431**:3804-3813 10.1016/j.jmb.2019.07.003.

856 30. Yuan Y, Ayinuola YA, Singh D, Ayinuola O, Mayfield JA, Quek A, Whisstock JC, Law RHP [...],
857 Castellino FJ. Solution structural model of the complex of the binding regions of human
858 plasminogen with its M-protein receptor from *Streptococcus pyogenes* (2019) *Journal of*
859 *Structural Biology* **208**:18-29 10.1016/j.jsb.2019.07.005.

860 31. Bober M, Morgelin M, Olin AI, von Pawel-Rammingen U, Collin M. The Membrane Bound LRR
861 Lipoprotein Slr, and the Cell Wall-Anchored M1 Protein from *Streptococcus pyogenes* Both
862 Interact with Type I Collagen (2011) *PLoS One* **6** 10.1371/journal.pone.0020345.

863 32. Barroso V, Rohde M, Davies MR, Gillen CM, Nitsche-Schmitz DP, Dinkla K, Chhatwal GS.
864 Identification of active variants of PARF in human pathogenic group C and group G streptococci
865 leads to an amended description of its consensus motif (2009) *International Journal of Medical*
866 *Microbiology* **299**:547-53

867 33. Dinkla K, Nitsche-Schmitz DP, Barroso V, Reissmann S, Johansson HM, Frick IM, Rohde M,
868 Chhatwal GS. Identification of a streptococcal octapeptide motif involved in acute rheumatic
869 fever (2007) *Journal of Biological Chemistry* **282**:18686-93

870 34. Brandt CM, Spellerberg B. Human Infections Due to *Streptococcus dysgalactiae* Subspecies
871 *equisimilis* (2009) *Clinical Infectious Diseases* **49**:766-772 10.1086/605085.

35. Xie O, Zachreson C, Tonkin-Hill G, Price DJ, Lacey JA, Morris JM, McDonald MI, Bowen AC [...], Tong SYC. Overlapping *Streptococcus pyogenes* and *Streptococcus dysgalactiae* subspecies *equisimilis* household transmission and mobile genetic element exchange (2024) *Nature Communications* **15** 10.1038/s41467-024-47816-1.

36. Singh B, Fleury C, Jalalvand F, Riesbeck K. Human pathogens utilize host extracellular matrix proteins laminin and collagen for adhesion and invasion of the host (2012) *FEMS Microbiology Reviews* **36**:1122-80 10.1111/j.1574-6976.2012.00340.x.

37. Arora S, Gordon J, Hook M. Collagen Binding Proteins of Gram-Positive Pathogens (2021) *Frontiers in Microbiology* **12** 10.3389/fmicb.2021.628798.

38. Zong Y, Xu Y, Liang X, Keene DR, Hook A, Gurusiddappa S, Hook M, Narayana SV. A 'Collagen Hug' model for Staphylococcus aureus CNA binding to collagen (2005) *EMBO Journal* **24**:4224-36 10.1038/sj.emboj.7600888.

39. Leo JC, Elovaara H, Bihan D, Pugh N, Kilpinen SK, Raynal N, Skurnik M, Farndale RW, Goldman A. First analysis of a bacterial collagen-binding protein with collagen Toolkits: promiscuous binding of YadA to collagens may explain how YadA interferes with host processes (2010) *Infection and Immunity* **78**:3226-36

40. van Wieringen T, Kalamajski S, Liden A, Bihan D, Guss B, Heinegard D, Farndale RW, Rubin K. The streptococcal collagen-binding protein CNE specifically interferes with alphaVbeta3-mediated cellular interactions with triple helical collagen (2010) *Journal of Biological Chemistry* **285**:35803-13 10.1074/jbc.M110.146001.

41. Tandon R, Sharma M, Chandrashekhar Y, Kotb M, Yacoub MH, Narula J. Revisiting the pathogenesis of rheumatic fever and carditis (2013) *Nature Reviews Cardiology* **10**:171-7 10.1038/nrcardio.2012.197.

42. Nitsche DP, Johansson HM, Frick IM, Mörgelin M. Streptococcal protein FOG, a novel matrix adhesin interacting with collagen I *in vivo* (2006) *Journal of Biological Chemistry* **281**:1670-1679 10.1074/jbc.M506776200.

43. Delorenzi M, Speed T. An HMM model for coiled-coil domains and a comparison with PSSM-based predictions (2002) *Bioinformatics* **18**:617-25 10.1093/bioinformatics/18.4.617.

44. Ricard-Blum S. The Collagen Family (2011) *Cold Spring Harbor Perspectives in Biology* **3** 10.1101/cshperspect.a004978.

45. Konitsiotis AD, Raynal N, Bihan D, Hohenester E, Farndale RW, Leitinger B. Characterization of high affinity binding motifs for the discoidin domain receptor DDR2 in collagen (2008) *Journal of Biological Chemistry* **283**:6861-8

46. Zhou NE, Kay CM, Hodges RS. Disulfide bond contribution to protein stability: positional effects of substitution in the hydrophobic core of the two-stranded alpha-helical coiled-coil (1993) *Biochemistry* **32**:3178-87 10.1021/bi00063a033.

47. Howes JM, Bihan D, Slatter DA, Hamaia SW, Packman LC, Knauper V, Visse R, Farndale RW. The recognition of collagen and triple-helical Toolkit peptides by MMP-13: Sequence specificity for binding and cleavage (2014) *Journal of Biological Chemistry* **289**:24091-24101 10.1074/jbc.M114.583443.

48. Holm L, Laiho A, Toronen P, Salgado M. DALI shines a light on remote homologs: One hundred discoveries (2023) *Protein Science* **32**:e4519 10.1002/pro.4519.

49. Abramson J, Adler J, Dunger J, Evans R, Green T, Pritzel A, Ronneberger O, Willmore L [...], Jumper JM. Accurate structure prediction of biomolecular interactions with AlphaFold 3 (2024) *Nature* **630**:493-500 10.1038/s41586-024-07487-w.

50. Hamaia SW, Pugh N, Raynal N, Nemoz B, Stone R, Gullberg D, Bihan D, Farndale RW. Mapping of potent and specific binding motifs, GLOGEN and GVOGEA, for integrin alpha1beta1

using collagen toolkits II and III (2012) *Journal of Biological Chemistry* **287**:26019-28 10.1074/jbc.M112.353144.

51. Bergsten H, Palma Medina LM, Morgan M, Moll K, Skutlaberg DH, Skrede S, Wajima T, Svensson M, Norrby-Teglund A. Adjunctive Rifampicin Increases Antibiotic Efficacy in Group A Streptococcal Tissue Infection Models (2021) *Antimicrobial Agents and Chemotherapy* **65**:e0065821 10.1128/AAC.00658-21.

52. Siemens N, Kittang BR, Chakrakodi B, Oppegaard O, Johansson L, Bruun T, Mylvaganam H, Group IS [...], Norrby-Teglund A. Increased cytotoxicity and streptolysin O activity in group G streptococcal strains causing invasive tissue infections (2015) *Scientific Reports* **5**:16945 10.1038/srep16945.

53. Pedchenko V, Kitching AR, Hudson BG. Goodpasture's autoimmune disease - A collagen IV disorder (2018) *Matrix Biology* **71-72**:240-249 10.1016/j.matbio.2018.05.004.

54. Reissmann S, Gillen CM, Fulde M, Bergmann R, Nerlich A, Rajkumari R, Brahmadathan KN, Chhatwal GS, Nitsche-Schmitz DP. Region Specific and Worldwide Distribution of Collagen-Binding M Proteins with PARF Motifs among Human Pathogenic Streptococcal Isolates (2012) *PLoS One* **7** 10.1371/journal.pone.0030122.

55. Tolken LA, Neufend JV, Oppegaard O, Methling K, Moll K, Redanz S, Katsburg MMD, Ali MQ [...], Siemens N. Streptokinase reduces Streptococcus dysgalactiae subsp. equisimilis biofilm formation (2024) *BMC Microbiology* **24**:378 10.1186/s12866-024-03540-w.

56. Davies MA, de Gier B, Guy RL, Coelho J, van Dam AP, van Houdt R, Matamoros S, van den Berg M [...], van Sorge NM. Synchronous emergence of Streptococcus pyogenes emm type 3.93 with unique genomic inversion among invasive infections in the Netherlands and England (2024) *medRxiv*:2024.06.20.24308992 10.1101/2024.06.20.24308992.

57. Skutlaberg DH, Wiker HG, Mylvaganam H, Group IS, Norrby-Teglund A, Skrede S. Consistent Biofilm Formation by *Streptococcus pyogenes emm 1* Isolated From Patients With Necrotizing Soft Tissue Infections (2022) *Frontiers in Microbiology* **13**:822243 10.3389/fmicb.2022.822243.

58. Liu H, Naismith JH. A simple and efficient expression and purification system using two newly constructed vectors (2009) *Protein Expression and Purification* **63**:102-11 10.1016/j.pep.2008.09.008.

59. Dinkla K, Talay SR, Morgelin M, Graham RMA, Rohde M, Nitsche-Schmitz DP, Chhatwal GS. Crucial role of the CB3-region of collagen IV in PARF-induced acute rheumatic fever (2009) *PLoS One* **4**:e4666

60. Raynal N, Hamaia SW, Siljander PR, Maddox B, Peachey AR, Fernandez R, Foley LJ, Slatter DA [...], Farndale RW. Use of synthetic peptides to locate novel integrin alpha2beta1-binding motifs in human collagen III (2006) *Journal of Biological Chemistry* **281**:3821-31

61. Delaglio F, Grzesiek S, Vuister GW, Zhu G, Pfeifer J, Bax A. NMRPipe: a multidimensional spectral processing system based on UNIX pipes (1995) *Journal of Biomolecular Nmr* **6**:277-93 10.1007/BF00197809.

62. Vranken WF, Boucher W, Stevens TJ, Fogh RH, Pajon A, Llinas M, Ulrich EL, Markley JL [...], Laue ED. The CCPN data model for NMR spectroscopy: development of a software pipeline (2005) *Proteins-Structure Function and Genetics* **59**:687-96 10.1002/prot.20449.

63. McCoy AJ, Grosse-Kunstleve RW, Adams PD, Winn MD, Storoni LC, Read RJ. Phaser crystallographic software (2007) *Journal of Applied Crystallography* **40**:658-674 10.1107/S0021889807021206.

64. Emsley P, Lohkamp B, Scott WG, Cowtan K. Features and development of Coot (2010) *Acta Crystallographica Section D* **66**:486-501 10.1107/S0907444910007493.

966 65. Murshudov GN, Skubak P, Lebedev AA, Pannu NS, Steiner RA, Nicholls RA, Winn MD, Long
967 F, Vagin AA. REFMAC5 for the refinement of macromolecular crystal structures (2011) *Acta*
968 *Crystallographica Section D* **67**:355-67 10.1107/S0907444911001314.

969 66. Chen VB, Arendall WB, 3rd, Headd JJ, Keedy DA, Immormino RM, Kapral GJ, Murray LW,
970 Richardson JS, Richardson DC. MolProbity: all-atom structure validation for macromolecular
971 crystallography (2010) *Acta Crystallographica Section D* **66**:12-21
972 10.1107/S0907444909042073.

973 67. Kaul R, McGeer A, Low DE, Green K, Schwartz B. Population-based surveillance for group A
974 streptococcal necrotizing fasciitis: Clinical features, prognostic indicators, and microbiologic
975 analysis of seventy-seven cases. Ontario Group A Streptococcal Study (1997) *American Journal*
976 *of Medicine* **103**:18-24 10.1016/s0002-9343(97)00160-5.

977 68. Johansson L, Thulin P, Sendi P, Hertzen E, Linder A, Akesson P, Low DE, Agerberth B, Norrby-
978 Teglund A. Cathelicidin LL-37 in severe Streptococcus pyogenes soft tissue infections in
979 humans (2008) *Infection and Immunity* **76**:3399-404 10.1128/IAI.01392-07.

980 69. Thenmozhi R, Balaji K, Kumar R, Rao TS, Pandian SK. Characterization of biofilms in different
981 clinical M serotypes of Streptococcus pyogenes (2011) *Journal of Basic Microbiology* **51**:196-
982 204 10.1002/jobm.201000006.

983